NGI Rapport / Report

Australian Government
Geoscience Australia

UNISDR Global Assessment Report 2015 - GAR15

Tsunami methodology and result overview

20120052-03-R
28 May 2014
Revision 1, 6 February 2015

Department of Industry
Minister for Industry: The Hon Ian Macfarlane MP
Parliamentary Secretary: The Hon Bob Baldwin MP
Secretary: Ms Glenys Beauchamp PSM

Geoscience Australia
Chief Executive Officer: Dr Chris Pigram
This paper is published with the permission of the CEO, Geoscience Australia

Geoscience Australia's participation in this study was funded by the Australian Department of Foreign Affairs and Trade.

Project

Project:	UN-ISDAR Global Assessment Report 2015 – GAR 2015
Report No.:	20120052-03-R
Report title:	Tsunami methodology and result overview
Date:	28 May 2014
Revision No./date:	1, 6 February 2015

Client

Client:	The United Nations Office for Disaster Risk Reduction – UNISDR
Client's contact person:	Andrew Maskrey
Contract reference:	Signed agreement dated 16 November 2012

For NGI

Project manager:	Farrokh Nadim
Report prepared by:	Finn Løvholt, Sylfest Glimsdal, Helge Smebye (NGI), Jonathan Griffin, Gareth Davis (Geoscience Australia)
Reviewed by	Carl B. Harbitz
Work also carried out by:	INGV Roma (Stefano Lorito, Roberto Basili), USGS (Eric Geist), URS Corporation (Hong Kie Thio), IPMA Lisbon (Maria Ana Baptista)

Main office:
PO Box 3930 Ullevål Stadion
NO-0806 Oslo
Norway

Trondheim office:
PO Box 1230 Pirsenteret
NO-7462 Trondheim
Norway

T (+47) 22 02 30 00
F (+47) 22 23 04 48

BIC No. DNBANOKK
IBAN NO26 5096 0501 281
Company No.
958 254 318 MVA

ngi@ngi.no
www.ngi.no

BS EN ISO 9001
Certified by BSI
Reg. No. FS 32989

Summary

The present report gives a brief overview of the tsunami hazard component of the Global Assessment Report 2015, involving a global hazard analysis. Tsunamis are infrequent events with the power to cause massive loss of life, large economic losses, and cascading effects from the destruction of critical facilities. Infrequent, but large and highly destructive tsunami events generally pose greater risk than the cumulative effect of smaller and more frequent events.

The work presented here is the first global scale probabilistic assessment of tsunami hazard. This report details the applied methodology and input parameters. The results of this assessment are tsunami inundation footprints for a suite of earthquake events, each with an associated probability of occurrence. These results are then used by CIMNE to undertake a probabilistic tsunami risk assessment, which is reported separately. However, to demonstrate some of the outcomes of the analysis, extracted Probable Maximum Losses (PML) from the risk calculations as a function of the return period are included for a limited list of countries. Among others, the results reveal that the predicted PML for a return period of 500 years for Japan closely corresponds to the losses due to the 2011 Tohoku earthquake and tsunami.

There are a number of limitations to this global scale assessment; the most important ones are related to the assumption of full seismic coupling as well as the use of simplified methods for estimating inundation and exposure. Further sources of uncertainties are reviewed within this report. It should be stressed that the results presented here should not be used for local scale hazard and risk assessment, or to inform any local scale disaster management activities. Rather, they are intended to provide a global perspective that allows broad comparison between different regions.

Contents

1 Introduction

This report describes the methods and underlying data contributing to a global tsunami risk assessment that forms part of the Global Assessment Report for 2015 (GAR15). It describes the hazard evaluation only, as the vulnerability and risk assessment is performed and reported separately by the International Centre for Numerical Methods in Engineering (CIMNE). Based on two previous global tsunami hazard assessments (UN-ISDR 2009; 2013), the GAR15 work is the third global analysis of tsunami hazard and risk. The first global scale tsunami hazard and exposure assessment was conducted for the UN-ISDR Global Assessment Report 2009 (UN-ISDR, 2009), and is also summarized by Løvholt et al. (2012a). GAR 2009 focussed on tsunami exposure due to low probability-high consequence events, and used an estimate of tsunami hazard for the 500-years return period. Emphasis was put on developing countries and therefore certain regions were omitted or not fully covered. In the second global scale tsunami hazard assessment conducted for the Global Assessment Report 2013 (GAR13) this work was continued, and a more complete global coverage of the tsunami exposure for the 500-years return period was accomplished. The GAR13 work also included exposure of critical facilities and preliminary use of Probabilistic Tsunami Hazard Assessment (PTHA) method for the 500-years return period for a selected area (South and South East Asia and the Southwest Pacific). Results are summarised in the UN-ISDR Global Assessment Report 2013 (UN-ISDR, 2013), elaborated by Løvholt et al. (2014), and also presented in Appendix B in this report.

As indicated above, the previous tsunami hazard assessment in GAR was based on quantifying intensity measures at a single return period, largely derived from scenario simulations. In the design of the tsunami sources, tectonic slip rates and parameter-magnitude scaling laws were utilized (Bird, 2003; Blaser et al., 2010). Tsunamis having long return periods (that is, exceeding at least several hundred years), are believed to dominate the risk (Nadim and Glade, 2006). Løvholt et al. (2014) argued that a 500-years return period may provide a reasonably rough lower bound timescale for risk driving events in many areas. However, a more complete estimate of global tsunami risk can be derived by integrating hazard components over different return periods, i.e. by undertaking a probabilistic hazard assessment. The joint risk assessment method employed for all hazards in GAR15 has set the requirement for probabilistic approaches to be used, and in this case, a Probabilistic Tsunami Hazard Assessment (PTHA) method is applied. We note however, that the 500-years scenario-based hazard map accomplished for GAR13 represents a first order approximation for the same return period using the fully probabilistic method. The GAR13 500-years return period hazard map is depicted in Figure 1.

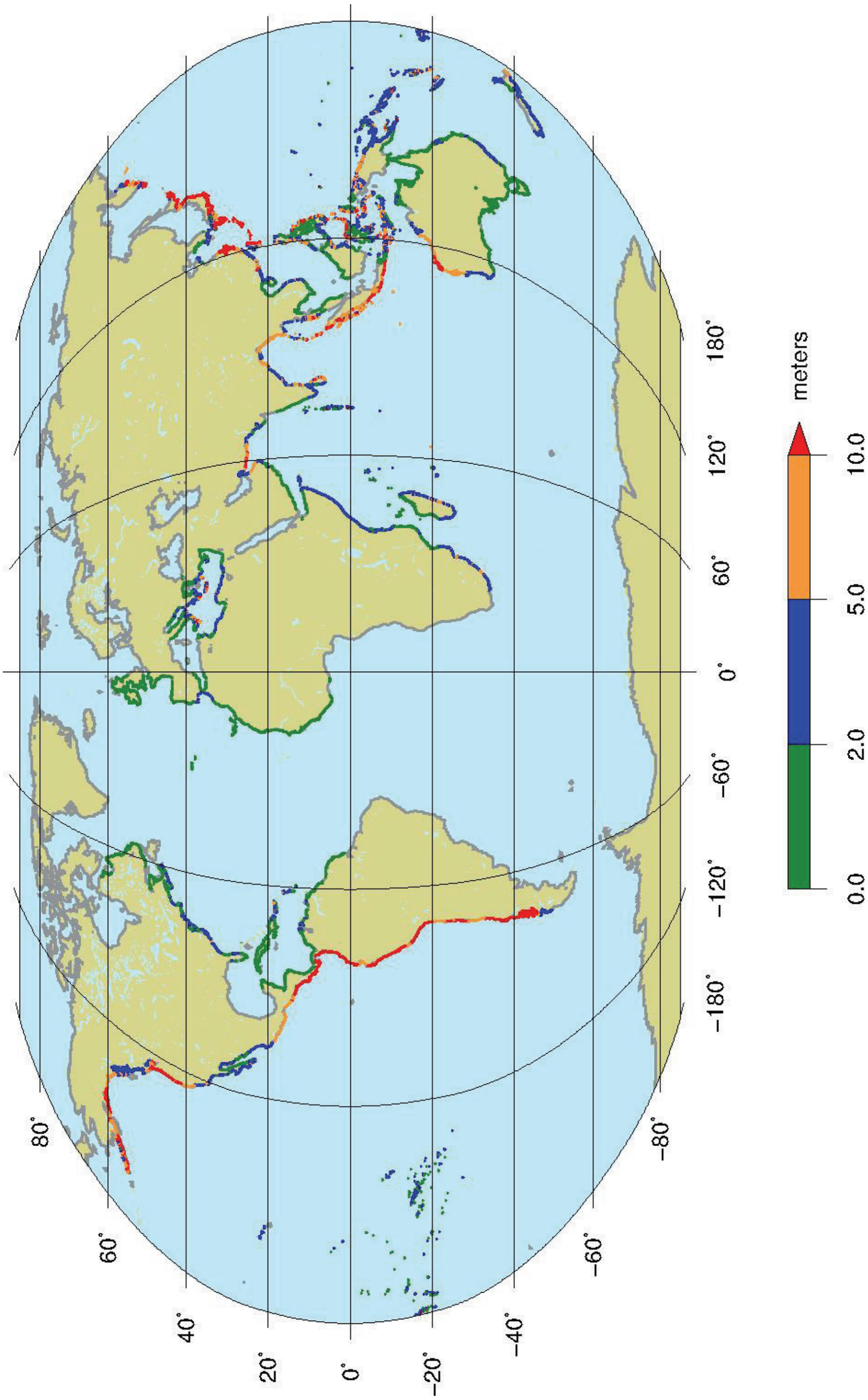

Figure 1: Global tsunami hazard based on scenarios for the GAR13 due to earthquakes for a 500-years return period. The colorbar gives the maximum shoreline water level in meters. We note that a similar aggregated map is not derived for GAR15 where a fully probabilistic approach is adopted.

For the above reasons, the PTHA method was selected for use in the GAR15 study. Modern PTHA methods are based on the model of Geist and Parsons (2006). In recent years, PTHA has been utilized to quantify the probability of the tsunami metric (usually the run-up height) in a number of areas (Annaka et al., 2007; Parsons and Geist, 2009; Gonzalez et al., 2009; Thio et al., 2010; Sørensen et al., 2012; Omira et al., 2014; Horspool et al., 2014; Lorito et al., 2014). Here, the PTHA method of Burbidge et al., (2008a,b) is combined with the method of amplification factors of Løvholt et al., (2012a) to estimate maximum shoreline water elevations; these maximum water elevations are in turn extrapolated to yield maximum run-up heights and inundation maps using public domain SRTM topographies. In GAR15, risk intensity measures such as the Annual Average Loss (AAL) and the Probable Maximum Loss (PML) are quantified by CIMNE. To facilitate the quantification of these terms, the PTHA was used to develop individual tsunami inundation maps for several thousand possible tsunami events with each event having an associated probability of occurrence. The applied methodology is elaborated below. The following points are stressed in relation to the GAR15 hazard assessment presented herein:

- Owing to the need for a global analysis, the proposed method for quantifying the tsunami hazard is based on simplifications and approximations, and is focusing on overall trends rather than details. The results of the study are hence a rough assessment of the tsunami hazard and population exposure.
- Earthquakes account for more than 80% of the tsunamis globally and therefore the focus of GAR15 is limited to earthquake-induced tsunamis. Tsunamis caused by submarine and subaerial landslides as well as volcanoes are not included in this study.
- The study focuses on tsunamis caused by large earthquakes only. The smallest subduction zone unit source in the present analysis has a moment magnitude (M_w) of 7.85.
- The hazard analysis is used to produce thousands of independent inundation maps with associated probability of occurrence, serving as input to the computation of the tsunami risk.
- The present report primarily discusses the hazard methodology, as another institution (CIMNE) carried out the risk assessment. Unlike previous GAR studies, an analysis of the tsunami hazard is omitted in the present report.

Due to the abovementioned reasons, the results will arguably involve significant uncertainties. As in common practice, we divide these into aleatory uncertainties (uncertainties inherent nature) and epistemic uncertainties (uncertainties due to lack of knowledge). We also note that the borderline between aleatory and epistemic uncertainties is sometimes obscure. Yet, these two terms are useful in our technical treatment of the uncertainties in the hazard assessment discussed in Section 2.1. Owing to the global scale of the analysis, yet several known factors that significantly influence on the accuracy of results were not straightforwardly captured in the analysis. Below, we briefly summarise the most important ones, and point out that these are discussed further in later parts of the report:

- **Uncertainties in earthquake magnitude-frequency (MF) distributions.** Large-magnitude earthquakes dominate the tsunami hazard. The large magnitude earthquakes are associated with sparse statistics and often involve magnitudes beyond the observational record. Therefore, we use tectonic information to derive return periods. As this is a poorly understood parameter, we assume full seismic coupling. *This is a conservative assumption with respect to the tsunami hazard.*
- **Representation of local earthquake sources.** The present analysis includes only sources aligned along major tectonic structures, mostly subduction zones. Hence, sources of more local character are not included. We also use the same value for the slip rate along each subduction zone, and therefore we do not include local spatial variations. *This may be locally under-conservative in certain regions where local faults are of importance for the tsunami hazard (for instance in the Mediterranean and eastern Indonesia).*
- **Other sources (landslides and volcanoes).** Only earthquake sources are included in this analysis, even though other sources comprise roughly 20% of the total. In low-seismic regions, landslide sources may totally dominate the tsunami hazard (Norway is a well-known example), and in these regions the estimated tsunami hazard from this report is not representative. *Omitting other sources is therefore an under-conservative assumption.*
- **Uncertainties in modelling the run-up height.** We calculate the run-up using a highly simplified model. The model assume plane wave evolution, and do not take into account local effects and wave breaking. We have partly taken into account the uncertainty in this model by incorporating a run-up uncertainty factor in our analysis. *Overall, the method provides conservative estimates of the tsunami run-up, but it may also provide too low estimates in certain situations.*

  Inaccuracies in topographical data and exposure calculations. For calculating the exposure, globally available SRTM data are used. Artefacts associated with the data may result in elevated land, and may wrongly prevent flooding. *Use of SRTM for representing the topography is one of the largest sources of uncertainties in the analysis; an under-conservative assumption.*

2 Methodology

The following sections provide details of the earthquake source models, tsunami simulations, method of amplification factors, and exposure calculations.

2.1 Employed Probabilistic Tsunami Hazard Assessment method

The PTHA approach describes the probability of exceedance for a given tsunami metric, and is derived from the well-established method of Probabilistic Seismic Hazard Assessment (Cornell, 1968) but adapted to account for tsunami propagation. Relatively recent studies have applied the PTHA method to different regions, e.g. Geist and Parsons (2006), Annaka et al. (2007), Burbidge et al. (2008a), Parsons and Geist (2009), and Thio et al. (2010). A short description of the employed PTHA method follows here, for a more complete description we refer to Horspool et al. (2014).

Standard PTHA methodology can be summarised as:

1. Define tsunami sources (earthquake faults) to be included in the analysis.
2. For each fault zone, discretise the fault into smaller sub-faults (unit sources).
3. For each source create a synthetic earthquake catalogue based on a recurrence model of choice (e.g. Gutenberg-Richter or Characteristic). The recurrence model relates magnitude to the probability of occurrence and is controlled by the slip-rate (convergence rate) at the source. Each synthetic event is a linear combination of adjacent sub-faults with the number of sub-faults and amount of slip dependent on the magnitude of the event. The same slip is applied to every sub-fault. For each magnitude, the full set of synthetic sources will cover the whole geometry of the subduction zones.
4. For each sub-fault, calculate the seafloor deformation for unit (1 m) slip and use this as the initial condition disturbance of the sea surface.
5. Propagate the resulting tsunami from source to hazard points offshore from the coastline of interest at a reference depth, using linear wave theory.
6. For each event in the synthetic earthquake catalogue, estimate the maximum water level at the near shore control point by summing the waves from all the individual sub-faults that make up that event, and then scale by the amount of slip for that event.
7. *Combine the maximum water level from all events from all source zones with the associated probability of each event to estimate the probability of exceedance.*

In the assessment presented here we do not complete step 7. Instead, from step 6 where we have a synthetic catalogue of tsunami events, we then:

1. Amplify near-shore tsunami water elevations to estimate maximum run-up height using the method of amplification factors (Løvholt et al., 2012a).
2. Estimate the inundation area for the event by applying the run-up height to the SRTM elevation dataset.

This results in a database of tsunami inundation events with associated probabilities that is then used for the GAR probabilistic tsunami risk assessment conducted by CIMNE.

The global PTHA analysis was split into two geographical domains:

1. The Indian and the Pacific Oceans; and
2. The Atlantic Ocean and Mediterranean Sea.

As large tsunamis can propagate between ocean basins, the domain overlapped and therefore a number of source regions were included in both.

2.2 Source models

As the largest earthquakes occur on subduction zones, only subduction zone sources were used for most regions. The exception was the Mediterranean, eastern Indonesia and North-East Atlantic regions where a few non-subduction sources were included, as these are considered regionally significant drivers of hazard. Key source parameters are summarised in Appendix A. Source traces are shown in Figure 2.

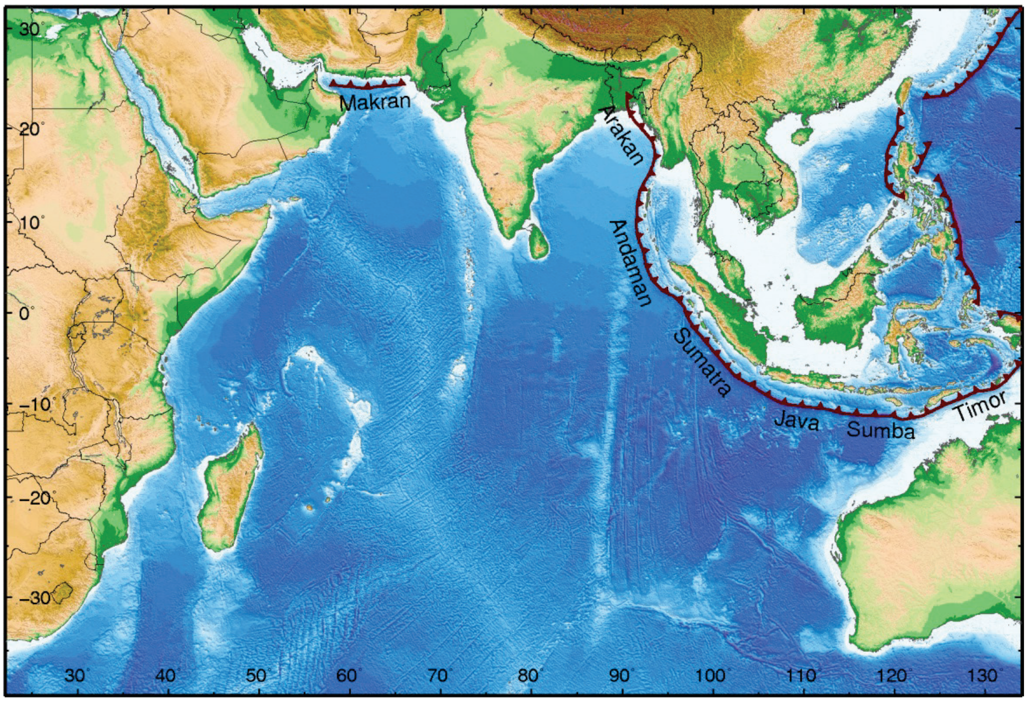

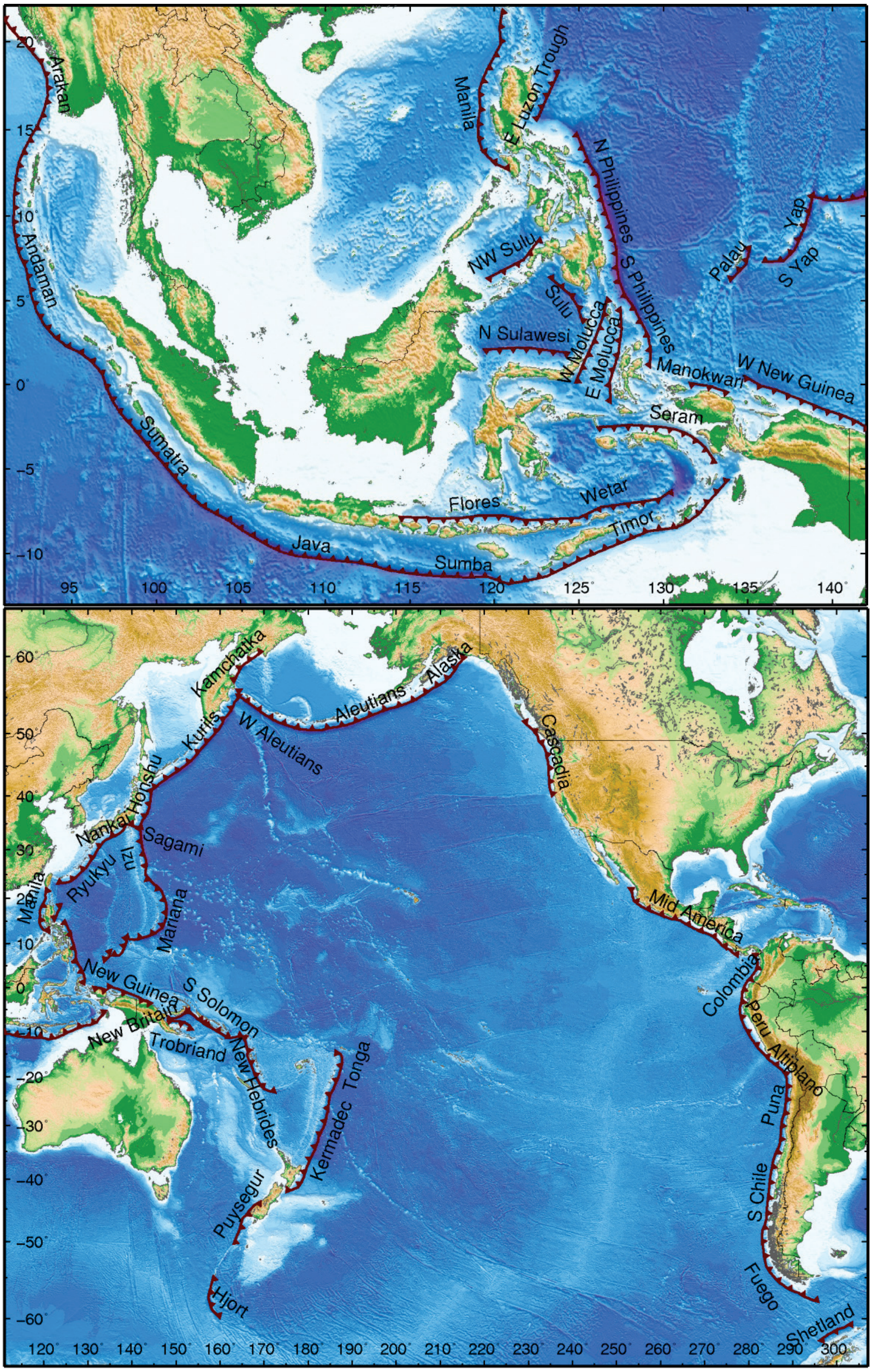
Arakan
Andaman
Sumatra
Java
Sumba
Flores
Wetar
Timor
Seram
Manila
E Luzon Trough
N Philippines
S Philippines
NW Sulu
Sulu
N Sulawesi
W Molucca
E Molucca
Manokwari
W New Guinea
Palau
Yap
S Yap
Kamchatka
Kurils
Honshu
Nankai
Sagami
Izu
Ryukyu
Manila
Mariana
New Guinea
New Britain
Trobriand
S Solomon
New Hebrides
Tonga
Kermadec
Puysegur
Hjort
Aleutians
W Aleutians
Alaska
Cascadia
Mid America
Colombia
Peru
Altiplano
Puna
S Chile
Fuego
Shetland

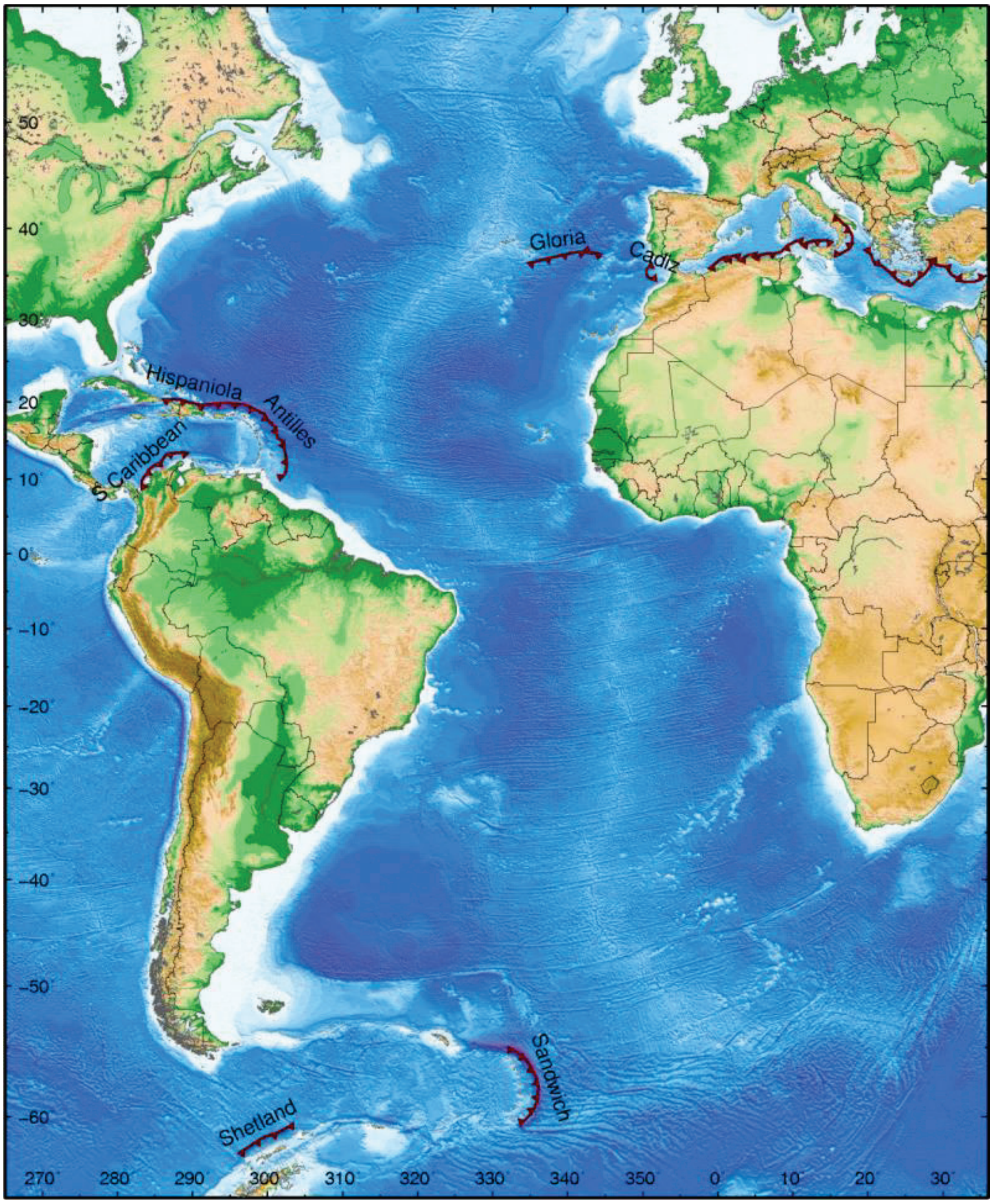
Gloria
Cadiz
Hispaniola
Antilles
S. Caribbean
Sandwich
Shetland
50°
40°
30°
20°
10°
0°
-10°
-20°
-30°
-40°
-50°
-60°
270°
280°
290°
300°
310°
320°
330°
340°
350°
0°
10°
20°
30°

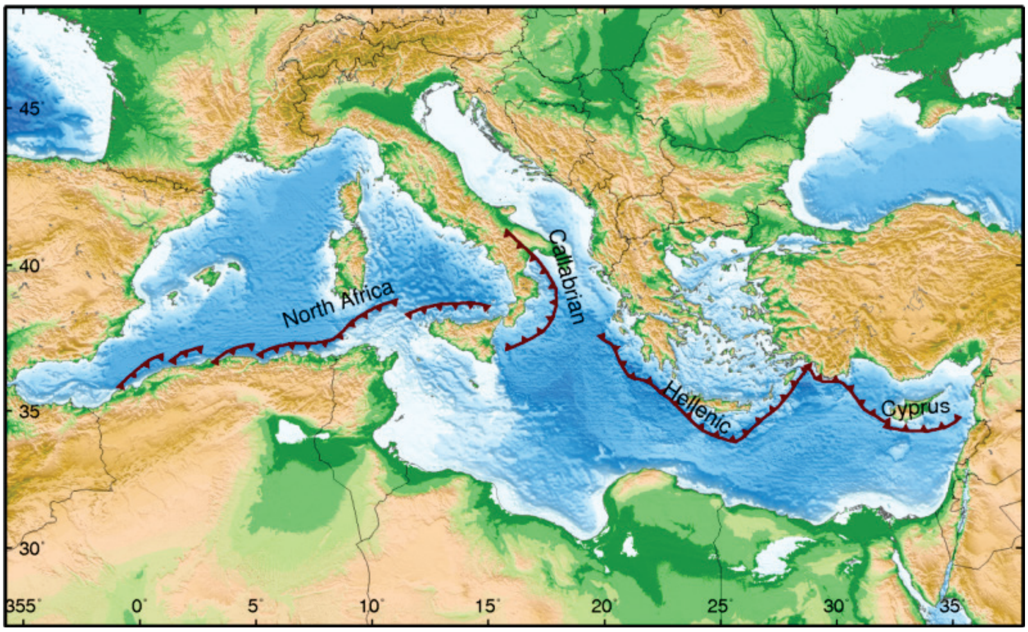

Figure 2: Source traces (in red) for a) the Indian Ocean region; b) South-east Asia; c) the Pacific Ocean region; d) the Atlantic Ocean region; and e) the Mediterranean region.

Subduction zone geometries and earthquake recurrence parameters were taken from: a combination of the Slab 1.0 model (Hayes et al., 2012) and the Global Earthquake Model (GEM) Faulted Earth Subduction Characterisation Project (Berryman et al., 2013); sources used for tsunami hazard assessment for Australia (Burbidge et al., 2008ab), Indonesia (Horspool et al., 2014), the north-east Atlantic (Matias et al., 2013; Omira et al., 2014), the Caribbean (Parsons and Geist, 2009); and source characterisation for the Mediterranean for the Seismic Hazard Harmonization in Europe (SHARE) project's European Database of Seismogenic Faults (Basili et al., 2013).

Subduction zone geometries are taken from Slab 1.0 (Hayes et al., 2012) where they exist. Where these geometries do not exist, source geometries for the Indian and Pacific Oceans are primarily taken from Burbidge et al. (2008a,b) and Horspool et al. (2014), both based on the plate boundaries of Bird (2003). Sources for the Indonesian region taken from Horspool et al. (2014) are modified from Bird (2003) based on Irsyam et al.'s (2010) earthquake source model. Source traces in the Caribbean are from Bird's (2003) model. Maximum depth of the seismogenic zone is taken as the maximum max_depth parameter from the GEM database (Berryman et al., 2013). We allow ruptures to propagate to the trench in all source regions except the Hellenic Arc, as in this region the trench is significantly further south (near the north coast of Africa) than the expected up-dip limit of the active megathrust.

For the Mediterranean Sea three subduction zones are defined based on the SHARE project, with the addition of the North Africa Thrust as this is considered significant for local tsunami hazard. For the NE Atlantic we include the only non-thrust source in our model, the Gloria Fault, which is a large transform fault that is a significant contributor to hazard in this region (Omira et al., 2014). In the Gulf of Cadiz we include one representative source zone that attempts to account for a number of thrust structures here that are too small to be well resolved if explicitly included in our model. All relative motion is applied to this fault for recurrence calculations.

Where the Slab 1.0 (Hayes et al., 2012) or SHARE (Basili et al., 2013) non-linear slab geometries do not exist, we use planar geometry extending the fault-plane down-dip from the fault trace. We discretise fault interfaces (whether planar or not) onto 5 km x 5 km ‘small’ sub-faults resulting in a high-resolution definition of the fault structure. The 5 km x 5 km sub-faults are then grouped into larger 100 km x 50 km ‘large’ sub-faults. For each large sub-fault the surface deformation resulting from a unit 1 m of slip on each of its component small sub-faults is calculated and aggregated; this deformation is then used as an initial condition to the tsunami propagation model. This process is illustrated in Figure 3. Through linear combinations, the large sub-faults then form the basis of the probabilistic analysis to create the synthetic event database. This approach allows us to resolve non-linear subduction interface geometries while maintaining a coarser approach to the grid size of our tsunami propagation calculations and reducing the complexity of our probabilistic calculations.

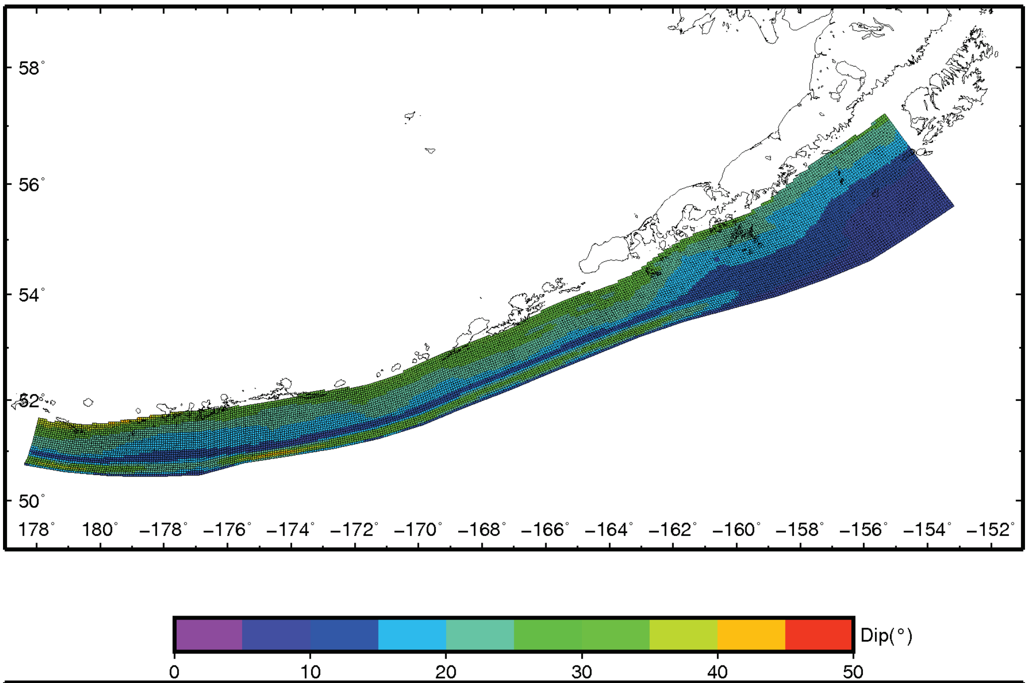
58°
56°
54°
52°
50°
178° 180° −178° −176° −174° −172° −170° −168° −166° −164° −162° −160° −158° −156° −154° −152°
Dip(°)
0 10 20 30 40 50

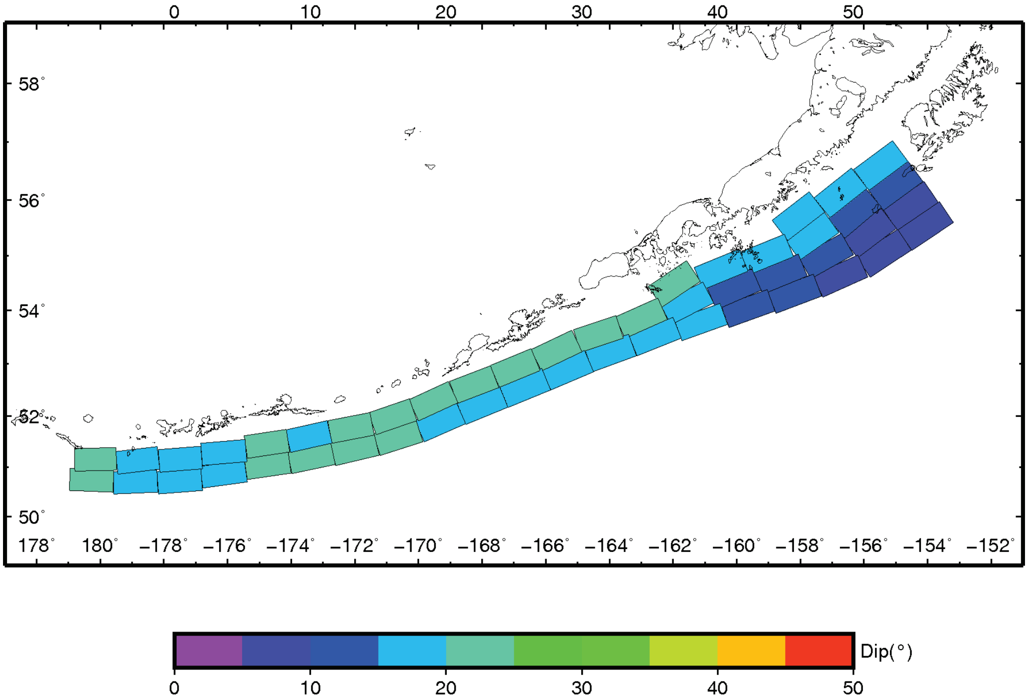
58°
56°
54°
52°
50°
178° 180° −178° −176° −174° −172° −170° −168° −166° −164° −162° −160° −158° −156° −154° −152°
Dip(°)
0 10 20 30 40 50

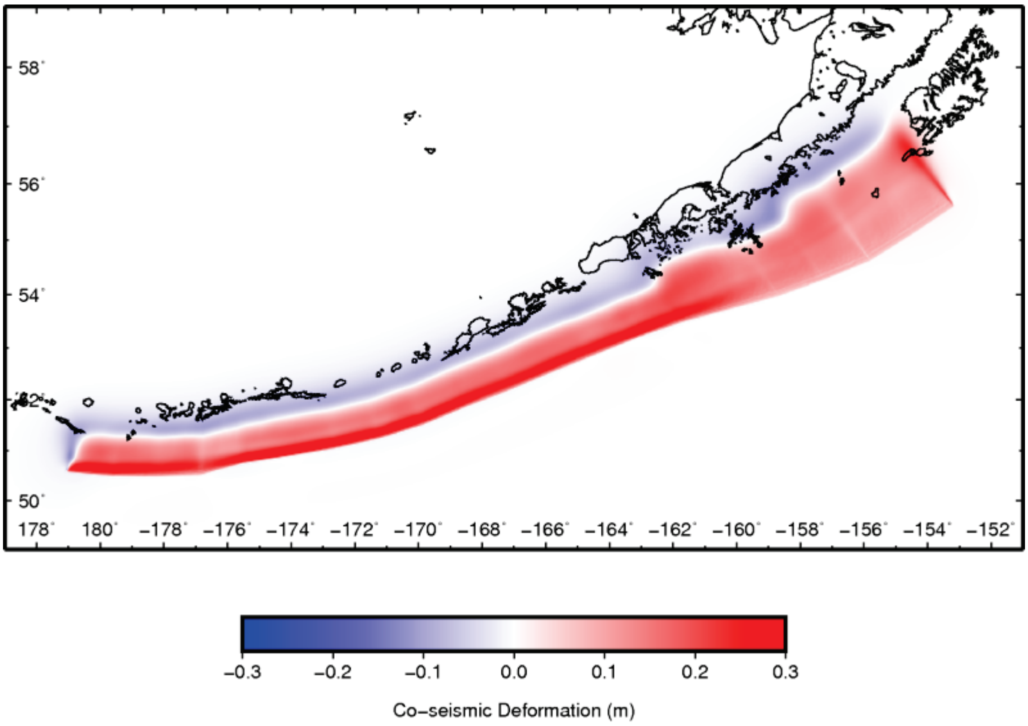

Figure 3: Illustration of development of source models for the Aleutians source zone showing a) 5 km x 5 km subfault model approximating the non-linear fault interface; b) 100 km x 50 km subfault model used as the basis of the probabilistic calculations; and c) surface co-seismic deformation for 1 m of slip on all component 5 km x 5 km subfaults of each large 100 km x 50 km subfault.

Surface deformation is calculated using the EDGRN code (Wang et al.,2003) and a layered crustal structure. We assume a generic layered earth model using Crust 1.0 continental arc structure (Table 1) (Laske et al., 2012). We note that the Crust 1.0 model includes a variety of relevant crustal structure classes, including forearcs, islands arcs, continental arcs, continental margins and ocean crust that overlap with the location of global subduction zones. We choose to uniformly apply the continental arc structure everywhere because:

a) Differences in calculated deformation between the models are small;
b) It gives greater deformation, and is therefore a more conservative choice, than island arc and forearc classes; and
c) The spatial resolution of the Crust 1.0 model is probably too coarse to accurately resolve spatial variations in crustal structure along subduction zone geometries (Gabi Laske, pers. comm. 2013), justifying use of a spatially uniform crustal structure.

Table 1: Crustal properties used for deformation calculations

Depth[km]	P-wave velocity [km/s]	S-wave velocity [km/s]	Density[kg/m^3]	Shear stiffness [GPa]
0.00	2.50	1.20	2.10	3
1.00	4.00	2.10	2.40	11
15.00	6.00	3.50	2.72	33
20.00	6.50	3.74	2.82	39
25.00	7.10	4.04	2.99	49
35.00	8.00	4.50	3.30	67

Recurrence parameters are primarily derived from the GEM subduction zone database (Berryman et al., 2013). Due to the computational and data management challenges of developing a full probabilistic suite of tsunami events at the global scale for risk assessment, we do not fully sample the range of epistemic uncertainty in the recurrence parameters provided in that report. Instead, we partially sample uncertainty through the use of a logic tree with the following approach:

a) We only consider a truncated Gutenberg-Richter (exponential) magnitude-frequency distribution. This model assumes a Poisson process where earthquakes are independent of each other.
b) The *preferred* maximum magnitude (*Mmax*) from the GEM database has a weight of 0.7 and the *maximum Mmax* a weight of 0.3. For sources that aren't in the GEM database we give reported *Mmax* a weight of 0.3 and arbitrarily assign a weight of 0.7 to *Mmax-0.1* magnitude units.
c) We assume full coupling everywhere (coupling coefficient = 1.0)
d) We use the preferred Gutenberg-Richter *b*-value from the GEM database.
e) We use the maximum slip-rate as defined below.

Recurrence parameters are summarised in Appendix A.

The segmentation of our source models does not always align with that in the GEM database, e.g. where we derived geometries from Burbidge et al. (2008b). Where one of our segments corresponds to more than one of the GEM segments, we take the most conservative recurrence parameters across all the GEM segments that overlap our source zone; i.e. maximum *Mmax*, minimum preferred *b*-value and maximum slip-rate. In most cases this does not introduce large deviations from the GEM model.

In addition, slip-rates vary along-strike. However, we apply a uniform slip-rate for each source region taking the maximum value reported along the full length of strike. In most cases differences are not large, with the exception of the Ryuku, Kermadec, Tonga, and New Hebrides trenches where there is a greater than 50 mm/year variation in slip-rate along-strike from one end of the fault to the other (Berryman et al., 2013). Therefore, for parts of these zones we may overestimate hazard. We do not attempt to resolve this issue in this assessment, but stress that this is a conservative assumption in some areas.

We assume pure thrust motion normal to the trench for all fault sources, with the exception of the Gloria Fault, which is strike-slip. This assumption is conservative and broadly valid for most sources regions, although there are some sources where slip is expected to be much more oblique, such as the Puerto Rico Trench (ten Brink, 2005).

2.3 Tsunami modelling

In deep water tsunami behaviour can be approximated by linear theory. This means that any tsunami can be constructed by the summation of the responses from multiple sub-fault sources. Hence, tsunami propagation simulations are only carried out once for each sub-fault, for 1 m of slip, and the hazard for each event is then determined by superposition of tsunami wave forms for the sub-faults with scaled slip that construct that event. A linear finite difference model (based on Satake, 1995) is used for simulation of tsunami propagation for the unit subfault sources. This solver is applied in spherical coordinates on a 1 arc-minute grid sampled from the GEBCO-08 global digital elevation model. Convergence testing for a limited number of sub-faults gives errors for the maximum wave height at hazard points that are generally < 25% (measured relative to model runs on a 30s GEBCO-08 grid) with no systematic bias although the largest errors tend to occur in regions of complex topography.

Hazard points are defined as the offshore points (or synthetic tide gauges) where the modelled tsunami is recorded. Hazard points are placed approximately along the 100 m depth contour at a spacing of 25 km, subject to constraints that they are not too near (< 1.5 arc-minutes) or too far (> 22 arc-minutes) away from the coastline; if this constraint is exceeded the hazard point is placed at the point within this constraint that is closest to 100 m depth. When hazard points are not situated at exactly 100 m depth, the wave height is normalised to 100 m using Green's law.

The earthquake event database is constructed by iterating through each magnitude in the magnitude-frequency distribution (in moment magnitude steps of 0.1) and calculating the rupture dimensions based on a scaling law (Strasser et al., 2010). The rupture is then iteratively moved across the fault until that magnitude has occurred on every possible location (i.e. every possible contiguous combination of sub-faults) within the fault dimensions. For M_W 7.85 earthquakes on the subduction interface, the rupture dimensions are equal to one sub-fault; therefore the number of ruptures would be equivalent to the number of sub-faults. This iterative process ensures that all magnitudes could occur at any possible location on the fault plane. For each event its probability is then the probability of that magnitude occurring on the fault divided by the number of earthquake events of that magnitude in the synthetic event database.

For each event in the synthetic catalogue, the tsunami hazard is calculated at each hazard point near the coast by summing the contributions from the scaled sub-faults that make up that event. For each site, this results in a list of tsunami events with maximum wave height and period, and the associated annual probability of the event.

Aleatory uncertainty in the PTHA comes from modelling uncertainties and inaccuracies, source geometry, and spatial and temporal variations in the slip. The aleatory uncertainty is roughly accounted for by employing a uniform logarithmic uncertainly of $\sigma = 0.3$, and is mostly based on previous modelling experience. For a discussion of incorporating uncertainties in PTHA, see Thio et al. (2010).

2.4 Run-up estimation and using amplification factors

To estimate tsunami run-up globally refined numerical inundation simulations are too time consuming. A faster procedure is to relate the near shore surface elevations at the hazard points to the maximum shoreline water levels by using a set of amplification factors based on the characteristics of the incident wave and the bathymetric slope. This procedure was developed for GAR 2009, and is described and validated in detail by Løvholt et al. (2012a), and only a part of the procedure is reviewed here.

The procedure is sketched in Figure 4. The amplification for a range of harmonic waves with different polarity and wave periods from a depth of 100 m to the shoreline is considered. The plane wave simulations are all run on idealized plane bathymetric configurations (see Løvholt et al., 2012a) where the shelf is broken up into two linear segments. From the plane wave simulations, factors for amplification that relate the surface elevation at time series gauges located at water depths of 100 m to the maximum shoreline water level are computed and stored in lookup tables.

To determine the amplification factors along the idealized bathymetric profiles we apply a linear hydrostatic plane wave model. The plane wave model utilizes grids of variable resolutions, allowing for finer grids in the shallowest waters. This enables more accurate results, fewer grid cells and less CPU time spent, and is also a necessity to resolve the waves in shallower waters during shoaling. In the plane wave simulations we therefore designed the grid to keep the Courant number equal to a constant value of 0.5. For the plane wave simulations a temporal increment of 2.5 s was employed, giving a spatial resolution ranging from 34 m close to the shoreline and 500 m in the deepest part. For smaller islands the plane wave assumption is severely violated, and therefore a 2HD model (depth averaged with two horizontal dimensions, Pedersen and Løvholt 2008, Løvholt et al. 2008) is applied. In the 2HD simulations, the spatial and uniform resolution was 1 arc min (about 1.85 km). The models apply a no-flux boundary condition at the shoreline leading to a doubling of surface elevation due to reflection. Although the models do not include dry land inundation, the surface elevation on the boundary close to the shoreline (at 0.5 m water depth) with a no-flux condition yields a good approximation. For long non-breaking waves, the linear solution for the water level at the shoreline and the non-linear solution for the run-up height on land are identical (Carrier and Greenspan, 1958). Based on Pedersen (2011), we may further assume that the procedure should also provide reasonably accurate results for waves of moderately oblique incidence. For reviews of different methods for run-up estimation, see Synolakis et al. (2007), Pedersen (2008), and Løvholt et al. (2013).

Figure 5 illustrates the amplification of the incoming wave as a function of the water depth. Waves with either a leading trough or a leading depression are considered. As expected, the shorter waves amplify most, and a leading depression gives more amplification, as described by Tadepalli and Synolakis (1996). We found that the amplification factor from a depth of 50 m ranges from nearly unity (steep slope combined with wide earthquake or earthquake located close to or partly on land) up to about 6 (very gentle slopes, e.g. profile 7 in Figure 5). In the first case, the wave is much longer than the distance from the control point to the shoreline, and hence both locations are influenced by the reflection at the shoreline at the same time. However, for shorter waves (i.e. short compared to the distance between the shoreline and the time series gauge) the amplification follows Green's law until the waves reach the shoreline and are doubled in height due to the reflection here (the reflection is not taken into account in Green's law). On the other hand, the amplification factors for small islands (with a diameter of same order or less than the wave length) with the same set of parameters are in the range 1-3. In the plane wave and 2HD model, the estimated maximum shoreline water elevation is measured close to the shoreline (at 0.5 m water depth).

To assign an amplification factor, an idealized bathymetric profile is manually assigned to each point, or to a section comprising a range of points with relatively similar cross-sectional depth profiles. To estimate the maximum shoreline water elevation from the offshore time series gauges in a tsunami simulation, the amplification factor for a set of parameters is extracted from the lookup tables and in turn multiplied with the maximum surface elevation measured at the hazard points.

The validation of the procedure is presented by Løvholt et al. (2012a), as well as by Løvholt and Glimsdal (2014). As an example, we list the validation by Løvholt and Glimsdal (2014) in Table 2, where we compare the simulated maximum inundation using the MOST model (Titov and Gonzalez, 1997) with the one obtained using amplification factors for the two Indian cities of Chennai and Nagapattinam. The comparison was conducted using five different scenarios originating from the Sunda Arc (Andaman and Sumatra trenches).

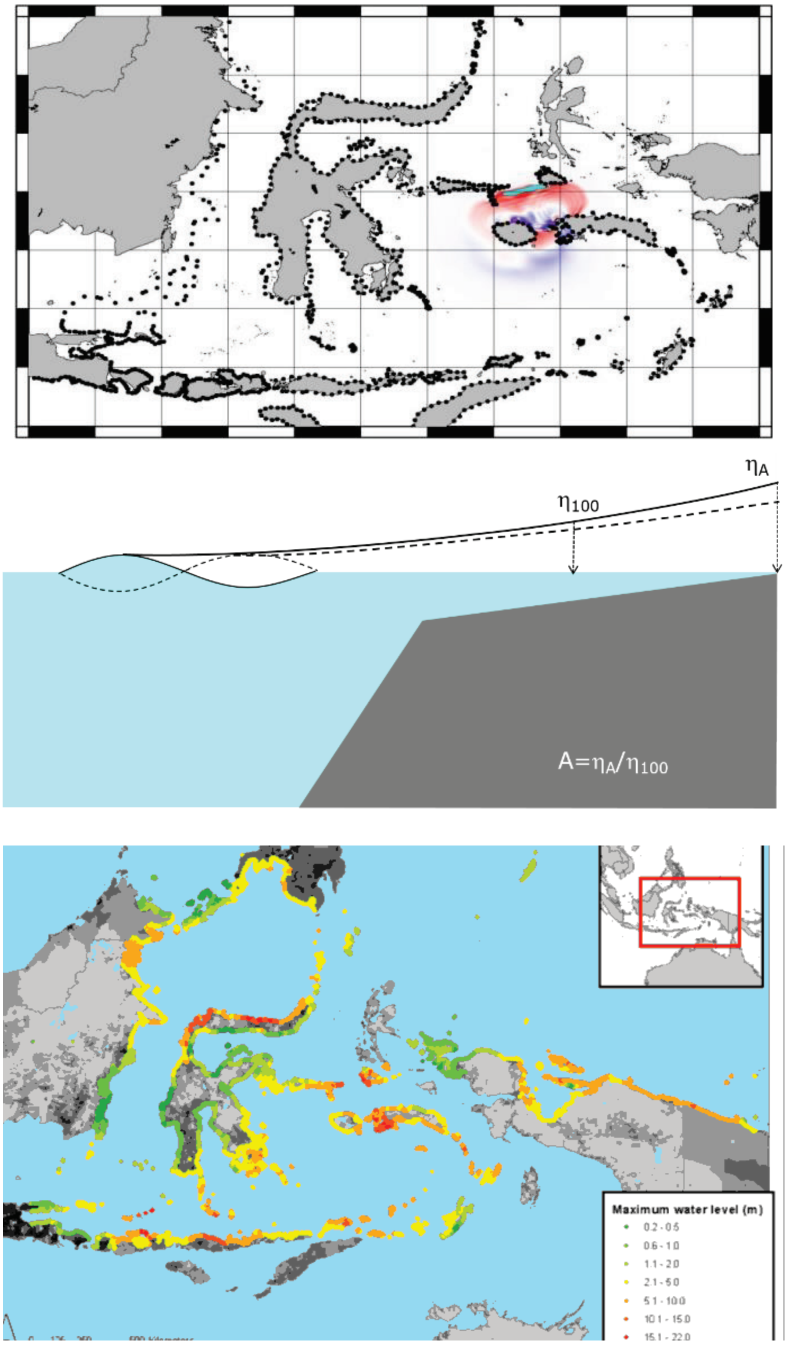

Figure 4: Principles of the amplification factor method. Upper panel, regional tsunami simulation and locations of the time series gauges at the 100 m depth contour. Mid panel, sketch of an idealized bathymetric profile. The amplification factor is defined as the ratio between the water surface elevation at the shoreline and the water surface elevation at 100 m water depth. Lower panel, maximum shoreline water level obtained from superimposing results from a series of simulations.

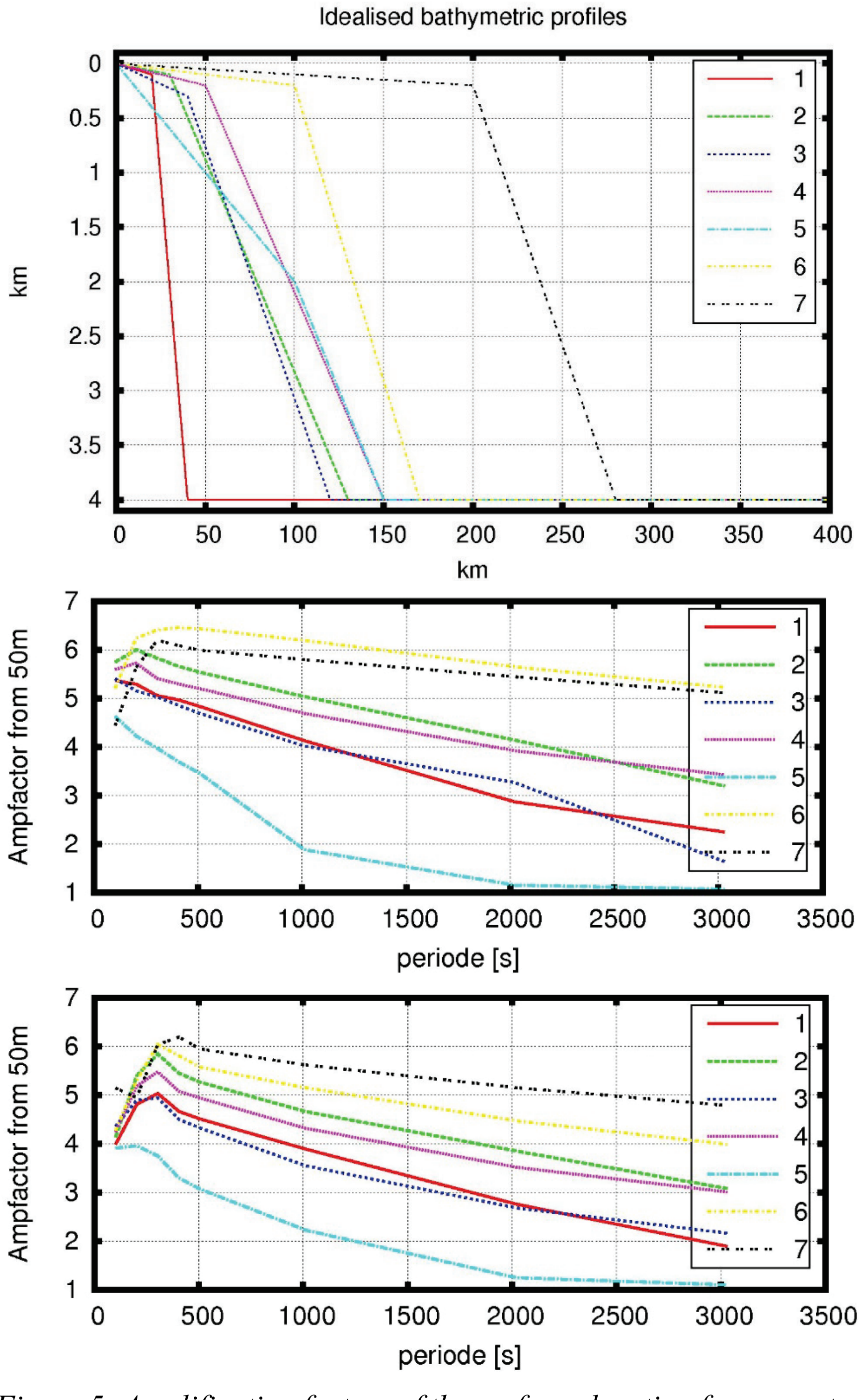

Figure 5: Amplification factors of the surface elevation from a water depth of 50 m and to the shore as a function of the incident wave period. Additional amplification from 100 m water depth is accounted by Green's law (an additional amplification factor of $2^{1/4}$). Upper panel, idealized profiles. Mid panel, amplification factors for a harmonic wave with leading trough. Lower panel, amplification factors for a harmonic wave with leading elevation.

Table 2: Comparisons of run-up calculations using amplification factors and the standard run-up model MOST. Comparisons are made for two locations, namely Chennai and Nagapattinam.

		Runup Chennai		***Runup Nagipattinam***	
Source location	***Mw***	***MOST***	***Amp factor***	***MOST***	***Amp factor***
Andaman	8.25	0,4	0,4	0,5	0,4
Andaman	8.75	1,8	1,7	1,9	2,0
Andaman	9.25	5,6	6,2	5,6	7,6
Sumatra	8.45	-	<0,3	0,2	<0.3
Sumatra	9.45	-	1,2	1,4	1,6

2.5 Inundation mapping and exposure

Based on the maximum shoreline water levels, inundation maps were computed in order to integrate the economic exposure to tsunami inundation. Due to the large number of scenarios, large calculation times were expected. Therefore, to reduce the calculation time, and because of the low vulnerability of exposure to water levels below 1 m, all water levels below 1 m were truncated to 0 and discarded in the calculations. The inundated area was computed by first interpolating the maximum water level between hazard points along the coastline contour. Next, we assume that the water level at the shoreline equals the maximum run-up, i.e. that the onshore water level is locally uniformly elevated over the mean sea level. An inverse distance weighted method was used to extrapolate the maximum water levels at the shoreline to the inland DEM, using the SRTM elevation dataset. For some very flat near shore locations, the inundation distance could be unreasonably long. Therefore, to limit unreasonable inundation, a crude formula taking into account the head loss due to bottom friction was used. We represent the wave at the shoreline by a constant maximum water level at the shoreline and choose a friction coefficient $f=10^{-3}$. By assuming a quadratic friction law and a constant drop of hydraulic head loss along the inundation path, a simple formula for constraining the maximum inundation distance L_{max} was obtained, equal to the ratio of the surface elevation to the friction:

$$L_{max} = \frac{\eta}{f}$$

In addition, the L_{max} was limited to a maximum distance of 10 km. All inundation points exceeding L_{max} using the interpolation schemes above are removed from the inundation dataset. All inundation calculations were conducted at the 90 m spatial resolution of SRTM.

For the representation of the hazard, a lognormal probability distribution of the overland flow depth was assumed. For a given (dry-land) cell, we then define the following lognormal probability density function for the flow depth H to be used for subsequent risk quantification:

$$P(H) = \frac{1}{\sigma \cdot H \cdot \sqrt{2\pi}} e^{\frac{-(\ln(H)-\ln(\overline{H}))^2}{2\sigma^2}}$$

Here, the mean flow depth $\overline{H}$ in a given cell is taken as *R-D*, *R* being the simulated run-up for a given scenario (set equal to the maximum water level at the shoreline) and *D* being the topographic altitude. The reason for choosing *H* as the tsunami metric, is that the vulnerability functions used to quantify economic losses due to building damage are solely based on *H*. In the final risk calculations, cell sizes for the vulnerable elements at risk (i.e. building types), are larger than the SRTM cells. Hence, as an impact metric, we use average flow depth over the number of wet cells inside the larger cell. In addition, we provide a saturation value for the large cell that is simply the number of wet SRTM cells over the total number of cells, meaning that only this fraction of the elements at risk are exposed (exposed elements at risk = saturation value times total elements at risk).

The results were aggregated down to 1/10 of this resolution (larger cells) to represent the cell sizes used for the global loss calculations by CIMNE. During the aggregation process, the mean maximum run-up for the aggregated pixels was calculated together with a saturation value representing the number of "wet" pixels as part of total number of pixels.

3. Results

Using the methods above, we have produced several thousand tsunamigenic earthquake sources with corresponding probabilities, tsunami scenarios, and inundation maps globally. In this work leading to the global tsunami hazard maps, hazard curves (relating tsunami run-up to the probability) have not been produced as the emphasis of GAR 15 is on quantifying Annual Average Losses (AAL) and Probable Maximum Losses (PML).

We limit the further presentation of results to exemplifying some propagation patterns (Figure 6) and inundation maps (Figure 7). In Figure 6, note that only the largest events result in transoceanic tsunami run-ups exceeding 1 m, justifying the focus on large earthquakes for the purposes of a global scale analysis. To assess the broader impact of this study, the reader are referred to the proceeding GAR 15 report and online data resources that have not yet been published when completing the present report.

Examples of calculated PML's for a brief list of selected countries are presented in Figure 8 (both relative to the total GDP and total PML in MUSD). A typical trend, that has also been reported in the previous GAR13 (Løvholt et al. 2014), is that the relative PML for Small Island States (SIDS) is often high. Another point is that the loss from the 2011 Tohoku tsunami was reported to 210 BN USD, while the 2004 Indian Ocean tsunami lead to an economic loss of 9.8 BN USD (www.emdat.be). For Japan, the PML curve gives a loss of 210 BN USD for a return period of 500 years, whereas a loss of 8.7 BN USD for a return period of 1500 years is found for Indonesia. Return periods for megathrust earthquakes for Japan are uncertain, but ballpark estimates have roughly indicated 500 years and upwards (Kagan and Jackson, 2013), which indicate that calculated losses agree well combining their estimated return period and loss observations from Japan. While this remarkable agreement for Japan is probably a coincidence, it indicates that computed losses at least might provide correct ballpark numbers. For Indonesia, we are not able to make a similar direct comparison, but notice that computed losses similar to the 2004 Indian Ocean tsunami are comparable to the loss due to the 2004 Indian Ocean tsunami for a return period of 1500 years.

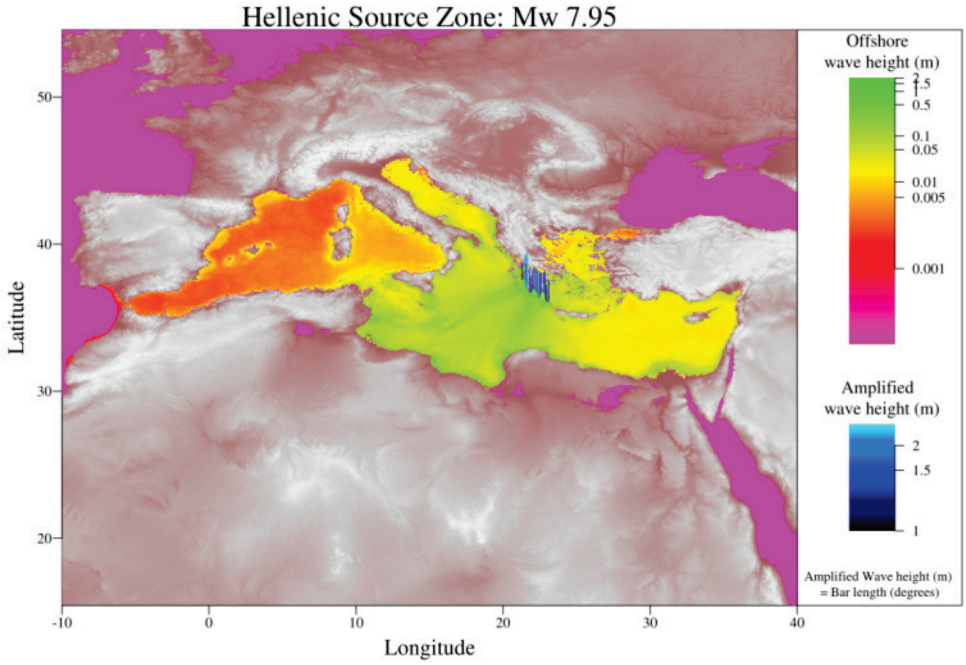
Hellenic Source Zone: Mw 7.95
Offshore wave height (m)
Amplified wave height (m)
Amplified Wave height (m) = Bar length (degrees)
Latitude
Longitude

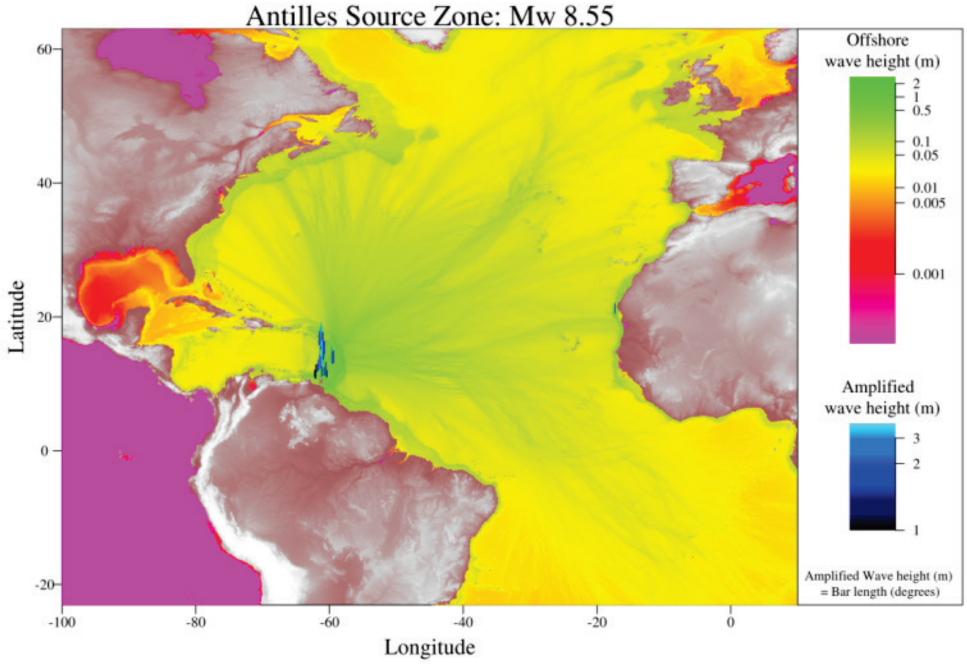
Antilles Source Zone: Mw 8.55
Offshore wave height (m)
Amplified wave height (m)
Amplified Wave height (m) = Bar length (degrees)
Latitude
Longitude

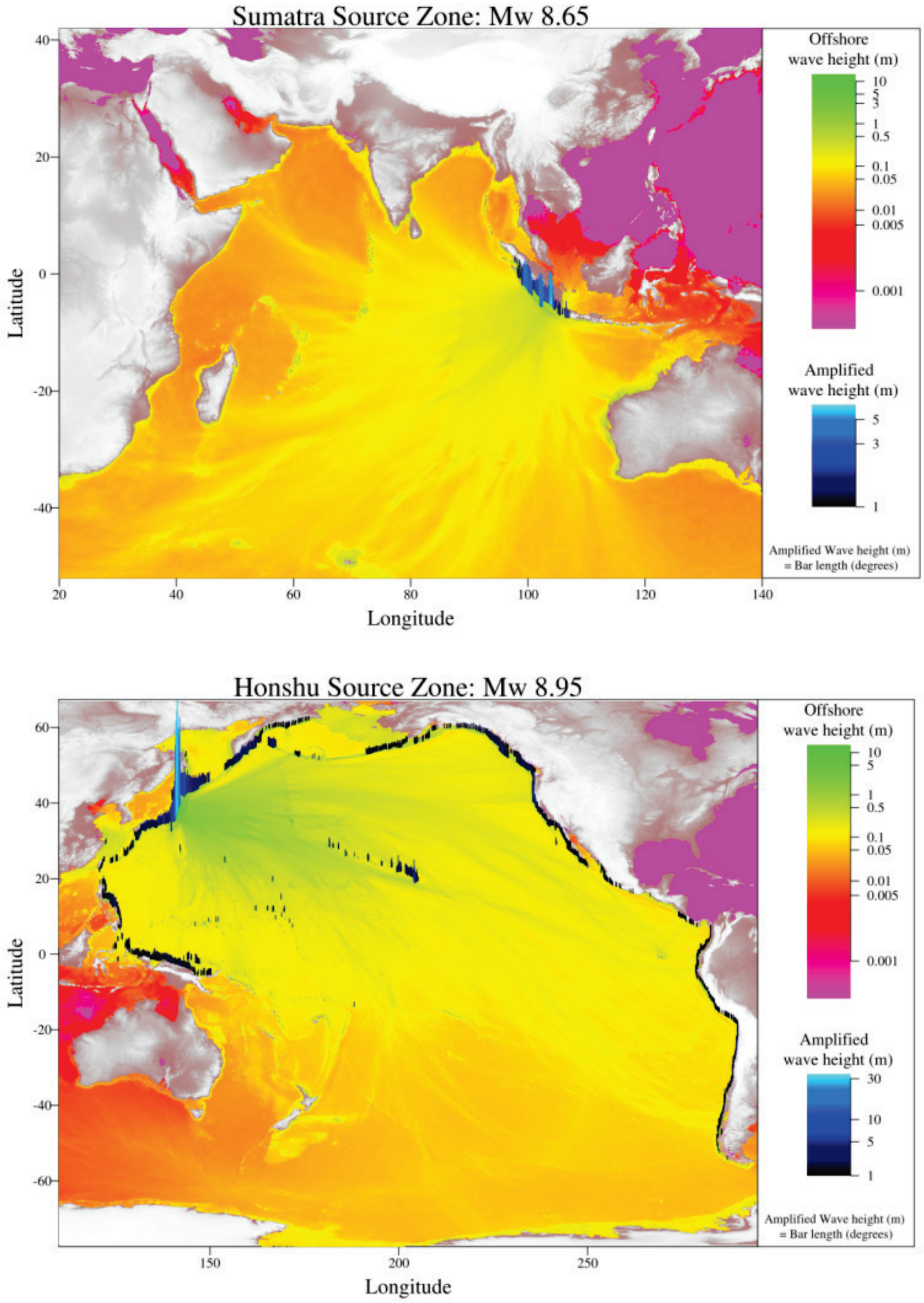

Figure 6: Example of simulated maximum water levels for different events from different source regions showing amplified run-up estimations (vertical bars) where run-up exceeds 1 m for a) Hellenic Arc; b) Lesser Antilles; c) Sumatra; and d) Honshu.

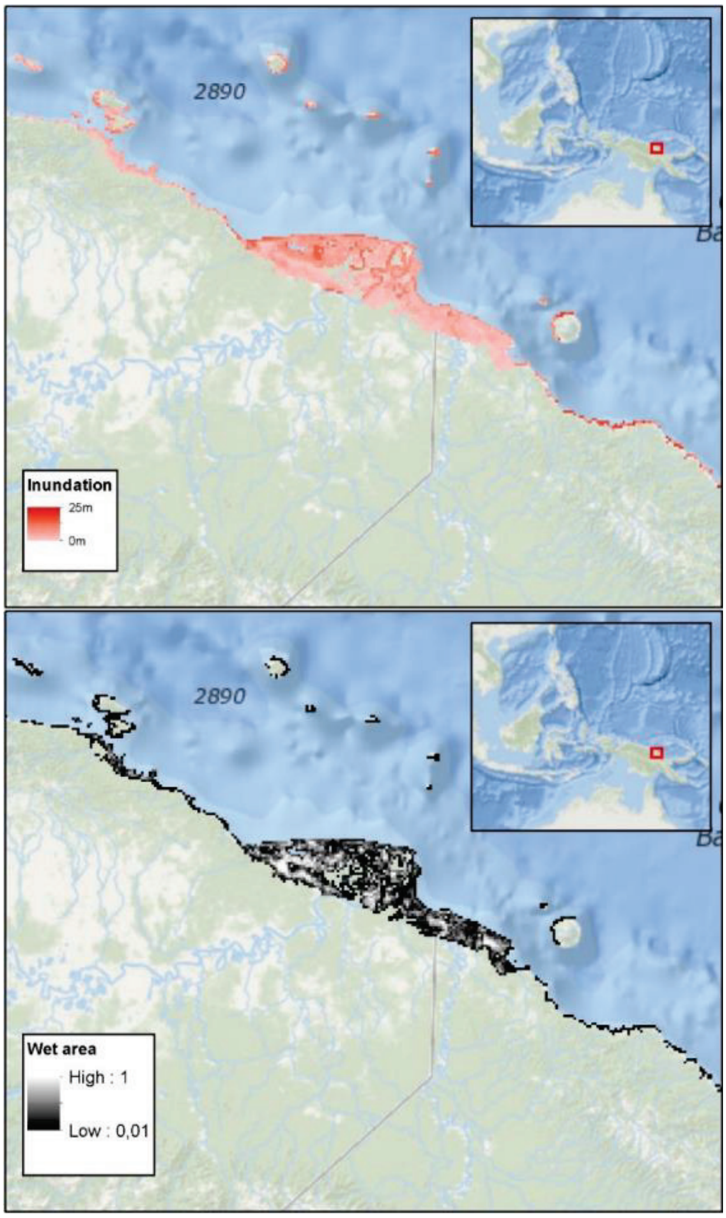

Figure 7: Upper panel: Example map of a simulated inundated area in Papua New Guinea with associated flow depths. Lower panel, saturation values covering the same area.

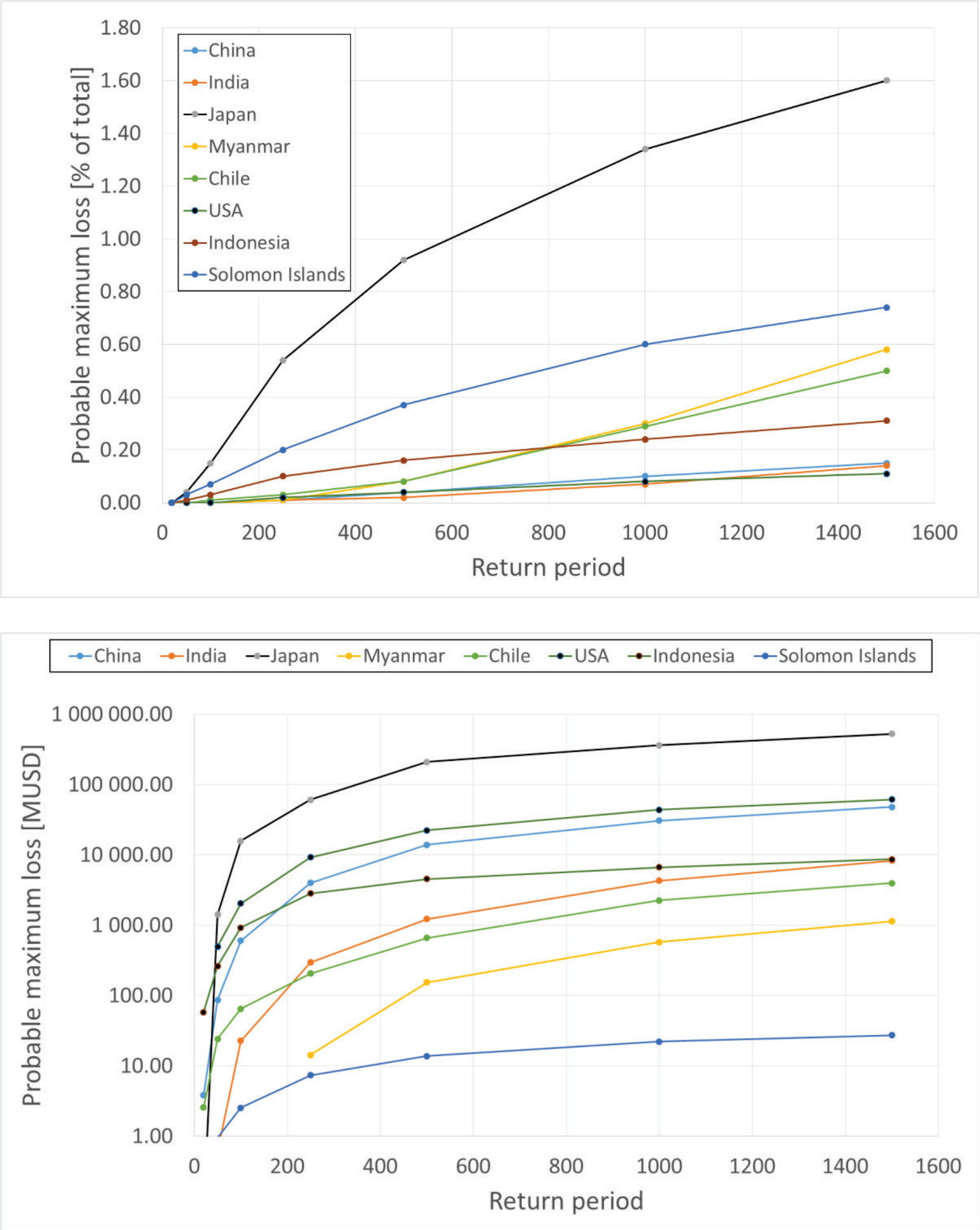

Figure 8: Selected probable maximum loss curves extracted from CIMNE's loss calculations. Upper panel, loss relative to the total exposed value for the whole country. Lower panel, probable maximum loss in MUSD. Missing data points indicate negligible losses (associated with short return periods).

4. Limitations, sources of error and look ahead

Due to the global nature of this study we expect relatively large uncertainties. Many of these uncertainties persist from previous analyses, which are discussed in Løvholt et al. (2012a, 2014). Some are simply uncertainties that may be incorporated by the standard deviation of the tsunami metric whereas others may involve systematic deviations that are less easily captured by adding larger uncertainties. Some bias is therefore expected. The most conservative assumptions are linked to tectonic assumptions, whereas the most under-conservative assumptions stem from the treatment of the inundation. We expect that the latter is the larger of the two. Using this argument, the tsunami hazard and risk estimates based on this study are expected to more likely underestimate than overestimate tsunami hazard. To this end, some different limitations of the study are outlined below.

4.1. Uncertainties related to tectonic information and return periods

The PTHA method incorporates a general weighting of different tectonic and seismic information in constraining the scenario parameters and return periods. The weighting involves judgement of the degree of tectonic coupling factors, shape of the magnitude-frequency distributions used, etc., where the amount of supporting data is sparse. As described in the methodology, there are some limits to the extent to which we sample recurrence uncertainty in the development of our synthetic scenarios. To this end, the assumption of full coupling is certainly conservative. We expect the uncertainty related to occurrence of large events to be particularly prominent, and in general the resulting return periods are clearly subject to uncertainty. We have introduced a uniform uncertainty measure that is clearly subjective, and would in general vary from region to region. This uncertainty to some extent takes into account the random variability due to heterogeneous slip distributions and uncertainties related to geometry information. The introduction of such a simple single-parameter measure of the uncertainty is obviously a simplification. Moreover, as lognormal distributions apply, a large uncertainty implies finite probabilities for large run-up. Another source of uncertainty is related to the shear stiffness that enters the seismic moment and therefore indirectly the return period. A uniform model for the stiffness due to layering is adopted, while we know that stiffness profiles are likely to vary spatially. In the present calculations, we may not be sufficiently conservative with respect to incorporating low stiffnesses which are associated with so-called tsunami earthquakes (see e.g., Kanamori 1972, for a discussion). Many important examples that are probable or almost certain slow events include Sanriku 1896, Aleutians 1946, Nicaragua 1992, Java 1994, Java 2006, and Mentawai 2010. Most of these events have magnitudes in the lower end of the magnitudes considered in our analysis. Therefore, the present analysis may be under-conservative with respect to tsunamis generated at lower magnitudes, particularly by slow rupturing near-trench earthquakes.

4.2. Omission of non-seismic sources

It should also be noted that tsunamis generated by non-seismic sources such as volcanoes, submarine and subaerial landslides, are not addressed in the present study. Non-seismic sources contribute to the generation of about one fifth of all tsunamis globally, and there are several examples of such tsunamis causing devastation. A recent example is the 1998 Papua New Guinea tsunami caused by a submarine landslide triggered by an earthquake, causing 2182 fatalities (source, http://www.emdat.be). In areas like eastern Indonesia (Løvholt et al., 2012b) and the Caribbean (Harbitz et al., 2012) tsunamis due to landslides and volcanoes are relatively more frequent, and contribute to a significant portion of the risk. Therefore, the tsunami hazard may be underestimated in such areas where landslides are more frequent. In Norway, where virtually all tsunamis are caused by landslides, the derived hazard maps based on earthquakes are not representative. It has also recently been claimed that large run-up in northern Japan following the 2011 Tohoku tsunami was induced by a huge submarine slump (Tappin et al., 2014). Unlike earthquakes, landslides are not constrained to the major subduction zones and may strike unexpectedly. Due to their source characteristics, landslides and volcanoes may generate larger run-up locally compared to earthquakes, but are generally less dangerous for the far-field propagation (for a discussion of their hazard, see e.g. Harbitz et al., 2013). However, addressing their return periods involves a larger scale of uncertainty than for earthquakes.

4.3. Interpretation of hazard maps and population exposure

Due to the extensive task of covering the whole world, emphasis is given to producing regional hazard maps and numbers for the subsequent risk analysis. The methods for establishing the hazard maps and population exposure are approximate and simplified in order to cover large geographical areas. They are not intended for detailed local hazard mapping, but rather to obtain regional and national data for comparison with other hazards. It should be noted that the inundation maps are based on coarse topographic data (SRTM) with low vertical accuracy including areas of falsely elevated land. Elevation uncertainties of the order of several metres in the SRTM dataset (Rodriguez et al., 2005) may exceed the height of many synthetic tsunamis included in this analysis. Griffin et al. (2012) showed how this may lead to a large underestimation of the inundation footprint and therefore an underestimation of the exposed elements. Løvholt et al. (2014) demonstrated that the sensitivity due to changes in the SRTM may be large (their results for a range of countries are presented in Table 3). By subtracting uniformly 2 m from the SRTM data, they found that the population exposure increases up to a factor 2 for Sri-Lanka, and a somewhat smaller factor for the other countries. Knowing that the SRTM data have a particularly positive bias in tropical and urban areas, we are led to the conclusion that the present exposure based on SRTM are lower-bound estimates. The effect is particularly pronounced in tropical areas (Römer et al., 2012), but may also play an important role in urban areas. Moreover, the effects of countermeasures such as breakwaters which are expected to decrease the exposure are not considered. Breakwaters are for instance common in Japan. In the hazard maps, differences in the reference location of the coastline sections sometimes occur. These differences may cause slight offsets between the affected zones and coastlines.

Table 3: Population exposure from GAR13 (500 years return period) for four different countries. The population exposure when uniformly subtracting 2 m from the topographic SRTM data is compared with the population exposure using pure SRTM data. Results are extracted from Løvholt et al., (2014).

	SRTM	SRTM - 2 m
Myanmar	253 000	312 000
Sri-Lanka	209 000	335 000
Pakistan	24 000	49 000
India	529 000	851 000

5. References

Annaka, T., Satake, K., Sakakiyama, T., Yanagisawa, K., and Shuto, N., (2007), Logic-tree approach for probabilistic tsunami hazard analysis and its applications to the Japanese coasts. *Pure Appl. Geophys*. 164, 577-92.

Baptista, M.A., Miranda, J.M., Batllo, J. and Macia, R. (2013), North-east Atlantic tsunamis related with Gloria Fault. *American Geophysical Union Fall Meeting Abstracts*.

Basili R., Kastelic V., Demircioglu M. B., Garcia Moreno D., Nemser E. S., Petricca P., Sboras S. P., Besana-Ostman G. M., Cabral J., Camelbeeck T., Caputo R., Danciu L., Domac H., Fonseca J., García-Mayordomo J., Giardini D., Glavatovic B., Gulen L., Ince Y., Pavlides S., Sesetyan K., Tarabusi G., Tiberti M. M., Utkucu M., Valensise G., Vanneste K., Vilanova S., Wössner J. (2013), The European Database of Seismogenic Faults (EDSF) compiled in the framework of the Project SHARE. http://diss.rm.ingv.it/share-edsf/, doi: 10.6092/INGV.IT-SHARE-EDSF

Berryman, K., Wallace, L., Hayes, G., Bird, P., Wang, K., Basili, R., Lay, T., Stein, R., Sagiya, T., Rubin, C., Barreintos, S., Kreemer, C., Litchfield, N., Pagani, M., Gledhill, K., Haller, K. and Costa, C. (2013), The GEM FaultedEarth Subduction Characterisation Project, [Version 1.0, June 2013, GEM Faulted Earth Project], available from http://www.nexus.globalquakemodel.org/gem-faulted-earth/posts .

Bird, P. (2003), An updated digital model of plate boundaries. Geochem. Geophys. Geosyst., 4(3): 1027, doi:10.1029/2001GC000252.

Blaser, L., F. Krüger, M. Ohrnberger, and F. Scherbaum (2010), Scaling Relations of Earthquake Source Parameter Estimates with Special Focus on Subduction Environment, *Bull. Seis. Soc. Am.*, 100, 2914-2926

Burbidge, D., Cummins, P.R., Mleczko, R., and Thio H.K. (2008a), A Probabilistic Tsunami Hazard Assessment for Western Australia, *Pure and Applied Geophysics*, DOI 10.1007/s00024-008-0421-x, 2008.

Burbidge, D., Mleczko, R., Thomas, C., Cummins, P., Nielsen, O., Dhu, T. (2008b). A Probabilistic Tsunami Hazard Assessment for Australia. *Geoscience Australia Professional Opinion. No.2008/04*

Carrier, G.F. and Greenspan, H.P. (1958), Water waves of finite amplitude on a sloping beach, J. Fluid Mech., 4 97-109

Cornell, C. A. (1968), Engineering seismic risk analysis, *Bull. Seismol. Soc. Am.*, 58, 1583–1606.

Geist, E. and T. Parsons (2006), Probabilistic analysis of tsunami hazards. *Nat. Hazards*, 37, pp. 277-314.

González, F.I., E.L. Geist, B. Jaffe, U. Kânoğlu, H. Mofjeld, C.E. Synolakis, V.V. Titov, D. Arcas, D. Bellomo, D. Carlton, T. Horning, J. Johnson, J. Newman, T. Parsons, R. Peters, C. Peterson, G. Priest, A. Venturato, J. Weber, F. Wong, and A. Yalciner (2009), Probabilistic tsunami hazard assessment at Seaside, Oregon, for near- and far-field seismic sources. *J. Geophys. Res.*, 114, C11023, doi: 10.1029/2008JC005132

Griffin, J.G., Latief, H., Kongko, W., Harig, S., Horspool, N., Hanung, R, Rojali, A., Maher, N., Fountain, L., Fuchs, A., Hossen, J., Upi, S., Dewanto, S.E., Cummins, P.R. (2012). An evaluation of onshore digital elevation models for tsunami inundation modelling. *American Geophysical Union Fall Meeting Abstracts*. http://fallmeeting.agu.org/2012/files/2012/12/Griffin-et-al-AGU-2012-NH21C-1598.pdf

Grilli S.T., Harris, J.C., Tajali Bakhsh, T.S., Tappin, D.R., Masterlark, T., Kirby, J.T., Shi, F., Ma, G., (2012), Recent progress in the nonlinear and dispersive modelling of tsunami generation and coastal impact: Application to Tohoku 2011, 13[èmes] Journées de l´Hydrodynamique, 21-23 November 2012, Chatou, France

Harbitz,C.B., S. Glimsdal, S. Bazin, N. Zamora, F. Løvholt, H. Bungum, H. Smebye, P. Gauer, O. Kjekstad (2012), Tsunami hazard in the Caribbean: Regional exposure derived from credible worst case scenarios. *Continental Shelf Research* 8, 1-23, doi:10.1016/j.csr.2012.02.006.

Harbitz,C.B., F. Løvholt, and H. Bungum (2013), Submarine landslide tsunamis – how extreme and how likely? *Nat. Hazards, in press*

Hayes, G. P., Wald, D. J., and Johnson, R. L. (2012), Slab1. 0: A three-dimensional model of global subduction zone geometries. *Journal of Geophysical Research: Solid Earth* (1978–2012), 117(B1).

Horspool, N., Pranantyo, I., Griffin, J., Latief, H., Natawidjaja, D. H., Kongko, W., Cipta, A., Bustaman, B., Anugrah, S. D., and Thio, H. K. (2014), A probabilistic tsunami hazard assessment for Indonesia, *Nat. Hazards Earth Sys. Sci.*, 14(11), 3105-3122

Irsyam, M., Sengara W., Aldiamar, F., Widiyantoro, S., Triyoso, W., Natawidjaja, D.H., Kertapati, E., Meilano, I., Suharjono, Asrurifak, M., and Ridwan, M., (2010)*, Development of Seismic Hazard Maps for Indonesia for Revision of Seismic Hazard Map in SNI 03-1726-2002.*

Kagan, Y.Y., Jackson, D.D. (2013), Tohoku earthquake: A surprise? *Bull. Seismol. Soc. Am.*;103 (2B): 1181–94

Kanamori, H. (1972), Mechanisms of Tsunami Earthquakes, Phys. Earth Planet. Interiors, 6, 346-359

Laske, G., Masters, G., Ma, Z., Pasyanos, M.E. (2012), CRUST1.0: An updated global model of Earth's crust. *Proceedings of the European Geosciences Union General Assembly 2012.*

Løvholt, F., Pedersen, G, and Gisler, G. (2008), Oceanic propagation of a potential tsunami from the La Palma Island, J. Geophys. Res., 113, C09026, doi:10.1029/2007JC004603

Løvholt, F., Glimsdal, S., Harbitz, C.B., Zamora, N., Nadim, F., Peduzzi, P., Dao, H., Smebye, H. (2012a), Tsunami hazard and exposure on the global scale, *Earth-Sci. Rev.*, 110, 1–4, 58-73, ISSN 0012-8252, 10.1016/j.earscirev.2011.10.002.

Løvholt, F., Kühn, D., Bungum, H., Harbitz, C.B., and Glimsdal, S. (2012b), Historical tsunamis and present tsunami hazard in eastern Indonesia and the southern Philippines, *J. Geophys. Res.*, 117, B09310, doi:10.1029/2012JB009425

Løvholt, F., Lynett, P., and Pedersen, G. (2013), Simulating run-up on steep slopes with operational Boussinesq models; capabilities, spurious effects and instabilities, *Nonlin. Processes Geophys.*, 20, 379-395, doi:10.5194/npg-20-379-2013

Løvholt, F., Glimsdal, S., Harbitz, C.B., Horspool, N., Smebye, H., de Bono, A., and Nadim, F. (2014), Global tsunami hazard and exposure due to large co-seismic slip, *Int. J. Disaster Risk Reduction*, ISSN 2212-4209, http://dx.doi.org/10.1016/j.ijdrr.2014.04.003.

Løvholt, F. and Glimsdal, S. (2014), Tsunami hazard assessment for Tamil Nadu – the Chennai and Nagapattinam cases, NGI report 20091887-00-5-R

Matias, L. M., Cunha, T., Annunziato, A., Baptista, M. A., and Carrilho, F.: Tsunamigenic earthquakes in the Gulf of Cadiz: fault model and recurrence (2013), *Nat. Hazards Earth Syst. Sci.*, 13, 1-13, doi:10.5194/nhess-13-1-2013, 2013

Nadim, F. and Glade, T. (2006), On tsunami risk assessment for the west coast of Thailand, F. Nadim, R. Pöttler, H. Einstein, H. Klapperich, and S. Kramer (Eds), ECI Symposium Series, 7. http://services.bepress.com/eci/geohazards/28, 2006.

Omira, R., Baptista, M.A., and Matias, L.. (2014), Probabilistic Tsunami Hazard in the Northeast Atlantic from Near- and Far-Field Tectonic Sources, *Pure App. Geophys.*, 1-20.

Parsons, T., and Geist, E., (2009), Tsunami probability in the Caribbean Region. *Pure App. Geoph.*, 165: 2089-2116

Pedersen, G., (2008), Modeling run-up with depth integrated equation models. *In Advanced Numerical Models for Simulating Tsunami Waves and Run-up*, Liu, P.L.-F., Yeh, H., and Synolakis, C. 3-41. World Scientific

Pedersen, G. and Løvholt F., (2008), Documentation of a global Boussiesq solver, Preprint series in Applied Mathematics, Department of Mathematics, University of Oslo, Norway, http://urn.nb.no/URN:NBN:no-27775

Pedersen, G. (2011), Oblique runup of non-breaking solitary waves on an inclined plane, *J. Fluid Mech.*, 668, 582–606, doi:10.1017/S0022112010005343.

Rodriguez, E. Morris, C.S., Belz, J.E., Chapin, E.C., Martin, J.M., Daffer, W. and Hensley, S. (2005), An assessment of the SRTM topographic products. Jet-Propulsion Laboratory D-31639. http://www2.jpl.nasa.gov/srtm/SRTM_D31639.pdf

Römer, H., Willroth, P., Kaiser, G., Vafeidis, A.T., Ludwig, R., Sterr, H. and Revilla Diez, J. (2012), Potential of remote sensing techniques for tsunami hazard and vulnerability analysis – a case study from Phang-Nga province, Thailand, *Nat. Hazards Earth Syst. Sci.*, 12, 2103-2126

Satake, K., (1995), Linear and non-linear computations of the 1992 Nicaragua earthquake tsunami. *Pure App. Geophys.,* 144, 455-470.

Strasser, F. O., Arango, M. C., & Bommer, J. J. (2010), Scaling of the source dimensions of interface and intraslab subduction-zone earthquakes with moment magnitude. *Seism. Res. Lett.*, 81(6), 941-950.

Synolakis, C.E. Bernard, E.N., Titov, V.V., Kânoglu, U., and Gonzaléz, F. (2007), Validation and Verification of Tsunami Numerical Models, *Pure Appl. Geophys.* 165, 2197–2228

Sørensen, M.B., Spada, M., Babeyko, A., Wiemer, S., Grünthal, G. (2012), Probabilistic tsunami hazard in the Mediterranean Sea, *J. Geophys. Res.*, 117, B1, 2156-2202, http://dx.doi.org/10.1029/2010JB008169

Tadepalli and Synolakis (1996), Model for the Leading Waves of Tsunamis, *Phys. Rev. Lett.* 77, 2141

Tappin, D.R., Grilli, S.T., Harris, J.C., Geller, R.J., Masterlark, T., Kirby, J.T., Shi, F., Ma, G., Thingbaijam, K.K.S., Mai, P.M. (2014), Did a submarine landslide contribute to the 2011 Tohoku tsunami?, *Marine Geology*, 357, 344-361

ten Brink, U. (2005), Vertical motions of the Puerto Rico Trench and Puerto Rico and their cause, *J. Geophys. Res*., 110, B06404, doi:10.1029/2004JB003459.

Thio H.K., Somerville P., and Polet J., (2010), Probabilistic Tsunami Hazard in California, *PEER Report 2010/108* Pacific Earthquake Engineering Research Center.

Titov, V.V. og Gonzalez, F.I. (1997). Implementation and testing of the Method of Splitting Tsunami (MOST) model. NOAA. Technical Memorandum ERL PMEL-112, 11 pp

UN-ISDR (2009), Global Assessment Report 2009, Risk and poverty in a changing climate, Invest today for a safer tomorrow, URL: http://www.preventionweb.net/english/hyogo/gar/2009/?pid:34&pif:3

UN-ISDR (2013), Global Assessment Report on Disaster Risk Reduction, From Shared Risk to Shared Value: The Business Case for Disaster Risk Reduction, ISBN 978-92-1-132038-1

Wang, R., Martín, F. L., and Roth, F. (2003), Computation of deformation induced by earthquakes in a multi-layered elastic crust—FORTRAN programs EDGRN/EDCMP. *Computers & Geosciences*, 29(2), 195-207

Appendix A - Table of fault parameters

Table A1 Fault parameters

Name	Maximum Depth[1] (km)	Slip-rate (mm/yr)	Maximum magnitude (Mw)	b-value
South Yap	45	7.1	8.83	0.54
Yap	45	9.0	8.93	0.8
Palau	45	7.1	8.83	0.54
Mariana	45	76.3	9.48	0.8
Izu	45	61.4	9.21	0.8
Ryukyu	25	134	9.09	0.8
Nankai	30	55.7	8.90	0.54
Sagami	30	36.0	8.42	1.0
Honshu	65	93.0	9.16	1.0
Kurils	60	90.9	9.73	1.0
Kamchatka	40	3.0	9.20	1.0
Western Aleutians	45	74.6	9.63	0.54
Aleutians	55	74.3	9.63	0.54
Alaska	50	58.4	9.20	0.8
Cascadia	30	47.8	9.20	0.54
Midamerica	35	79.1	9.23	1.0
Colombia	60	60.9	9.49	0.8
Peru	60	70.0	9.88	0.8
Altiplano	60	70.0	9.88	0.8
Puna	60	80.5	9.49	0.8
South Chile	60	80.5	9.53	0.8
Fuego	45	21.3	9.45	0.54
Sandwich	45	84.1	9.01	1.0
Shetland	45	10.0	8.71	0.8
Hjort	25	25.2	8.36	0.8
Puysegur	45	36.6	9.07	0.54
Kermadec	35	98.1	9.42	0.54
Tonga	45	269.5	9.17	1.0
New Hebrides	40	174.9	8.70	1.0
South-east Solomon	60	98.1	9.09	1.0
South Solomon Woodlark	60	98.1	9.09	1.0
South Solomon	60	107.0	8.62	1.0
New Britain	50	160.0	8.82	1.0

[1] Minimum depth of the seismogenic zones is the sea-floor at the trench for all sources except the Hellenic Arc, where ruptures do not propagate above 15 km depth.

Trobriand	50	13.0	9.2	1.0
East New Guinea	45	92.6	8.9	0.8
West New Guinea	45	28.1	9.03	0.8
Manokwari	45	21.8	8.64	0.8
North Sulawesi	45	51.6	8.89	0.8
East Molucca	30	28.0	8.7	1.0
West Molucca	45	16.5	8.47	0.8
North-west Sulu	45	19.4	8.72	0.8
Sulu	45	18.8	8.38	0.8
South Philippines	45	43.0	9.3	0.8
North Philippines	45	43.0	9.3	0.8
Manila	45	97.8	8.9	0.54
East Luzon Trough	45	14.2	8.38	0.8
Seram	45	74.2	9.04	0.8
Wetar	45	35.4	9.38	0.8
Flores	30	28.0	8.3	1.0
Timor	45	35.4	9.38	0.8
Sumba	40	69.3	9.42	0.54
Java	40	69.3	9.42	0.54
Sumatra	50	55.7	9.4	0.8
Andaman	45	50.8	9.55	0.54
Arakan	50	23.0	9.55	0.83
Makran	40	19.5	9.33	0.54
Sandwich	45	84.1	9.01	1.0
Antilles	45	20.1	9.37	0.54
South Caribbean	30	19.0	9.0	0.54
Hispaniola	45	20.0	9.37	0.54
Hellenic	45	35.0	9.0	1.17
North Africa	50	1.7	8.0	1.0
Callabrian	60	5.0	9.0	1.0
Cyprus	50	18.0	9.0	1.0
Cadiz	50	3.6	8.75	0.97
Gloria	60	4.0	8.75	1.0

Appendix B - GAR13 tsunami hazard assessment

Contents

B1 Introduction

The size of recent large scale tsunamis in Sumatra 2004 and Tohoku 2011 was to a large degree unexpected, changing our perspective on how to deal with high consequence - low probability events (Stein and Okal, 2007). The first global scale tsunami hazard and exposure assessment was conducted for the UN-ISDR Global Assessment Report 2009 (GAR, 2009), and is also summarized by Løvholt et al. (2012a). GAR 2009 focussed on tsunami exposure due to low probability-high consequence events. Emphasis was put on developing countries as certain regions were omitted or not fully covered.

Here, the methodology and results for the GAR 2013 report are outlined. The recent 2011 Tohoku earthquake and tsunami lead to an increased focus on impact of natural hazards on critical facilities. This is also reflected in the objectives of the GAR 2013 report. This event, among others, has led to the following objectives for the GAR 2013 report:

- Owing to the need for a global analysis, the proposed method for quantifying the tsunami hazard is based on simplifications and approximations, and is focusing on overall trends rather than details. The results of the study are hence a first-pass assessment of the tsunami hazard and population exposure.
- A primary objective in GAR 2013 is to provide a more complete coverage of earthquake tsunami sources globally to properly account for the exposure of population and critical facilities also in the industrialized countries in addition to previous focus regions from GAR 2009. Emphasis has been given to near field effects of tsunamis as these generally provide the larger run-up and shorter evacuation times.
- In order to obtain better statistics, a closer and more systematic sampling of offshore control points for run-up and exposure calculations has been conducted.
- Earthquakes account for more than 80% of the tsunamis globally and therefore the focus of GAR 2013 is limited to earthquake induced tsunamis. Tsunamis caused by landslides, rock slides, and volcanoes are not included in this study.
- The study focuses on tsunamis caused by large earthquakes only, as the largest events contribute more to the risk than the smaller events (Nadim and Glade, 2006).
- The design of new earthquake scenarios for GAR 2013 is constrained by the subduction zone convergence rate, conservatively assuming fault locking over 500 years. This gives a more formalized procedure for selecting the scenario earthquakes, as detailed below.

B2 Methodology

The objective is to produce global hazard maps and statistics of the exposure of elements at risk. The present report focuses on the population exposure and critical facilities. The tsunami inundation and exposure are obtained for a single return period of 500 years (close to a 10% exceedence probability in 50 years). Reliable estimates of the hazard at such large return periods are not easily established, particularly given the geographical extent of the problem and various sources of error and uncertainty. Hence, the return period is indicative to the order of magnitude only. Exposed areas are obtained by intersecting the modelled inundation with population density maps (Landscan, 2007) and economical values located in tsunami-prone areas in order to compute the exposure. To obtain such maps, scenario simulations are widely applied, to a large degree adopting the scenario methodology applied by Løvholt et al. (2012a), partly replacing previous results from GAR 2009, but also expanding the study area. Literature results are retained from GAR 2009 for New Zealand (Berryman et al., 2005) and Kamchatka (Kaistrenko et al., 2003), similarly earthquake scenario simulations covering the subduction zones offshore South America and along the Philippine and Manila trenches. Furthermore, results applied using probabilistic methods (PTHA, see e.g. Geist and Parsons, 2006; Thio et al., 2010) are used for certain areas. The various methods are briefly described below.

B2.1 Design of the earthquake scenarios

The considered earthquake scenarios are confined to those with the potential for tsunami generation due to co-seismic dip-slip motion. A compilation of all the scenarios are given in Figure 1. New scenarios cover eastern Indonesia, the Philippine trench and the northern Manila trench (Figure 2), northwards along the Ryukyu trench, the Nankai trough to the Japan trench (Figure 3). In the eastern Pacific new scenarios along the Aleutian trench and Cascadia trenches are provided (Figure 4). Previous scenarios from GAR 2009 for South America and new scenarios covering the Puerto Rico trench are depicted in Figure 5. For Europe potential earthquake scenarios offshore Portugal and the Eastern Mediterranean, including Sicily, the Adriatic Sea, and the Hellenic Arc are provided (Figure 6). A final set of scenarios are provided for the Makran trench south of Pakistan and Iran (Figure 7). Results for the South and South East Asia and the South West Pacific were obtained by the more elaborate PTHA method described below. The PTHA method combines relatively small unit sources for a range of subduction zones, these are not displayed below.

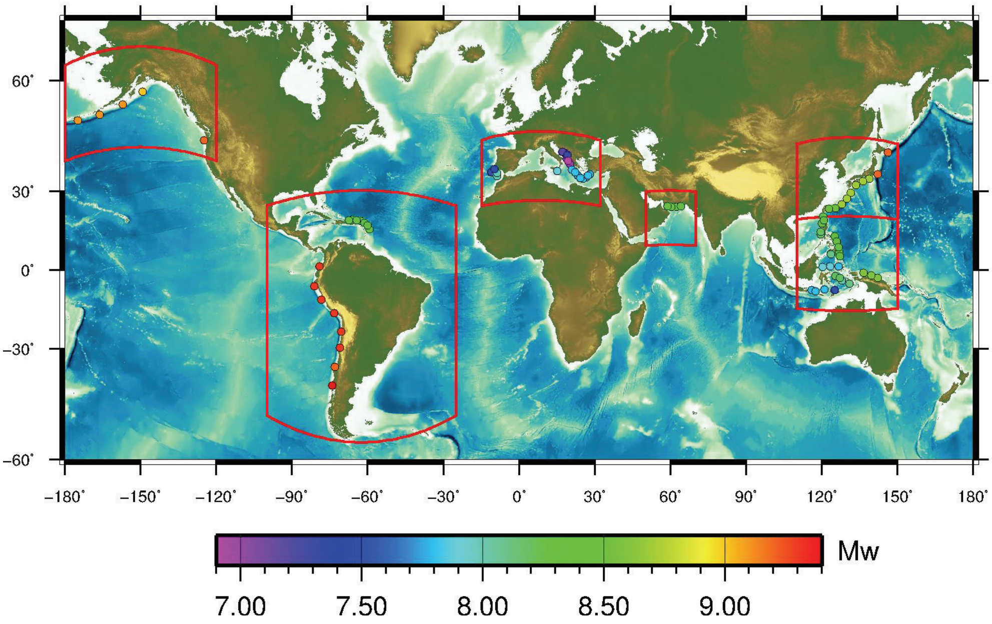

Figure B1 *Overview of the locations of the new employed scenarios in the present study. The red boxes depict areas presented below. The coloured dots represent the moment magnitudes and scenario locations. It is noted that for the Indian Ocean and south western Pacific, the PTHA is employed. The many PTHA unit sources are not displayed.*

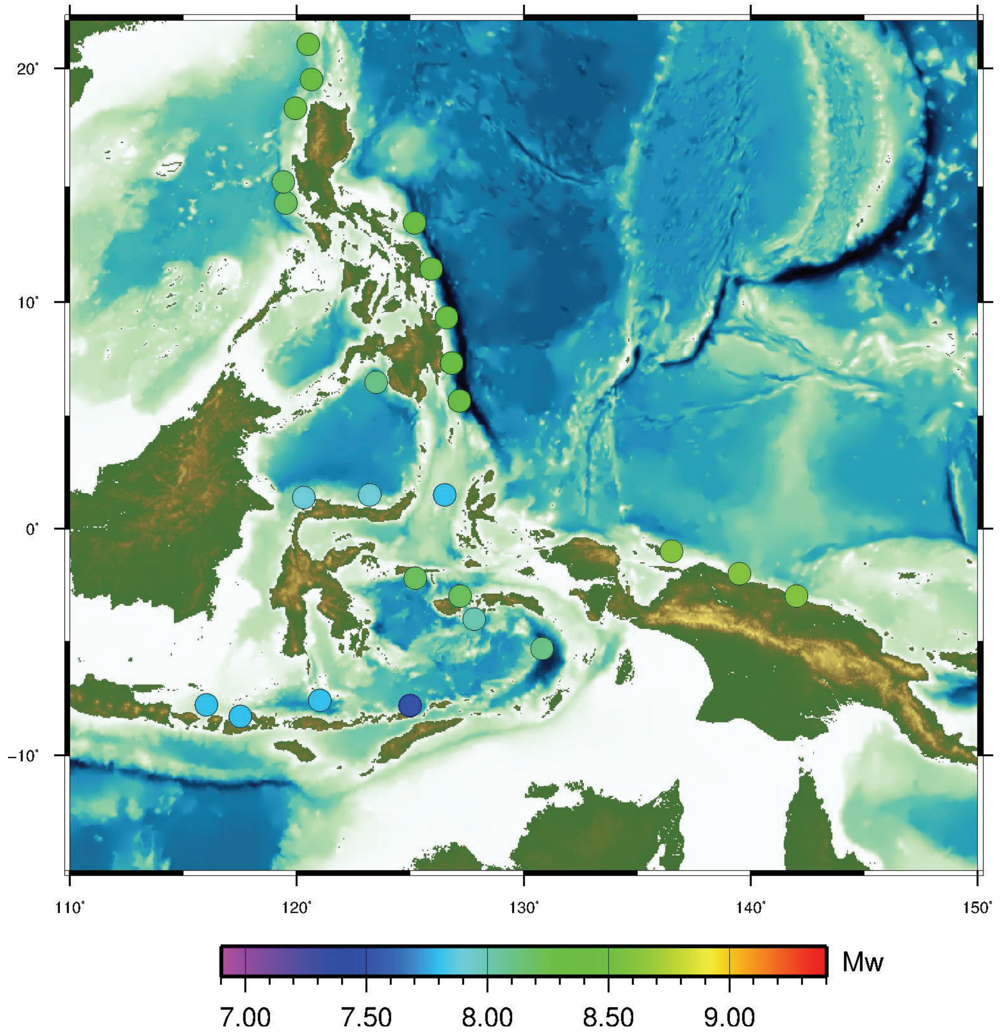

Figure B2 *Scenarios located in eastern Indonesia, the Philippines and New Guinea*

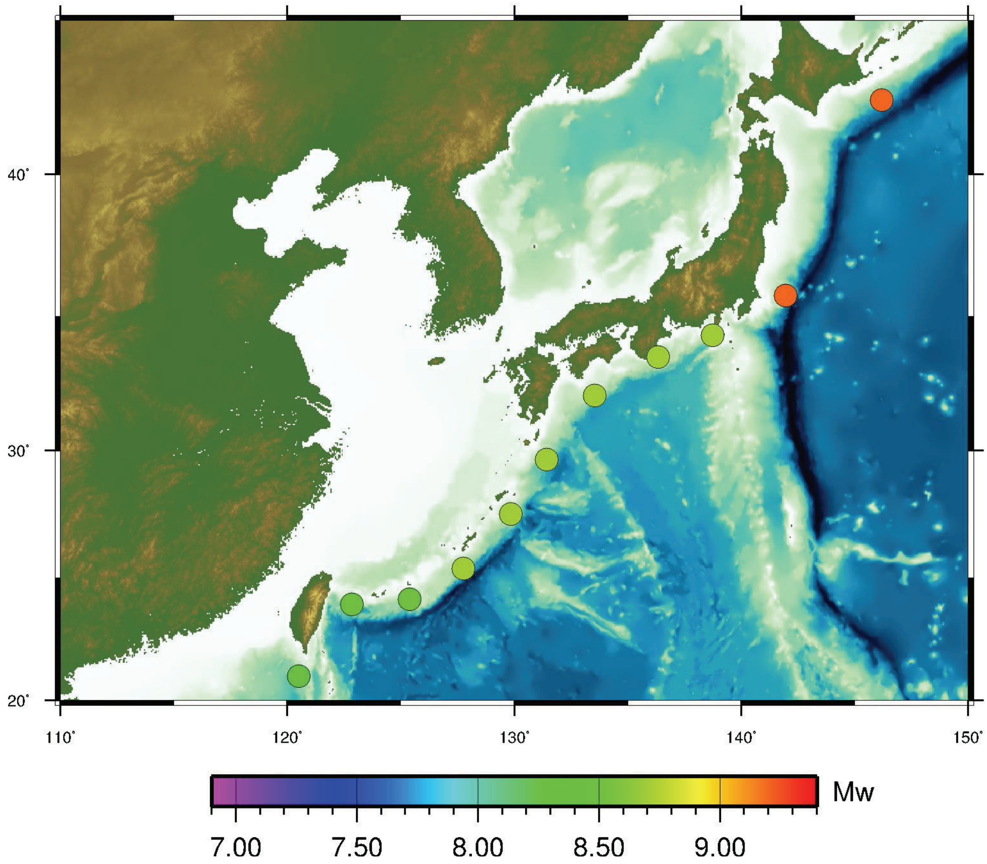

Figure B3 *Megathrust scenarios located along the Ryukyu trench, the Nankai trough, and the Japan trench.*

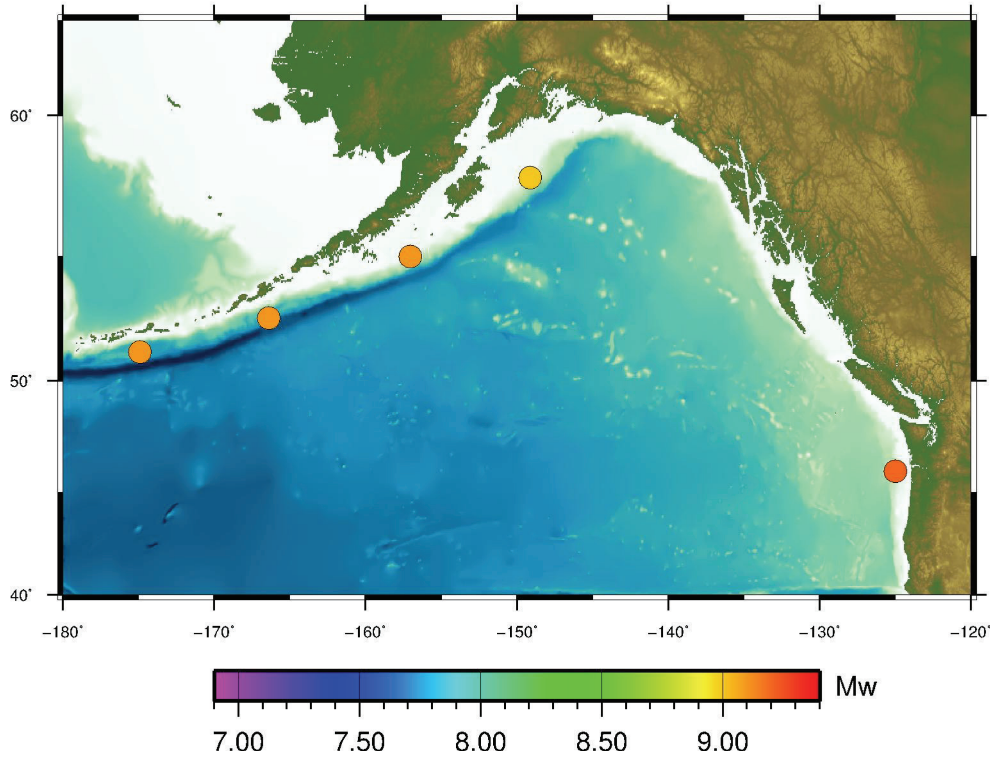

Figure B4 *Megathrust scenarios located along the Aleutean and Cascadia subduction zones*

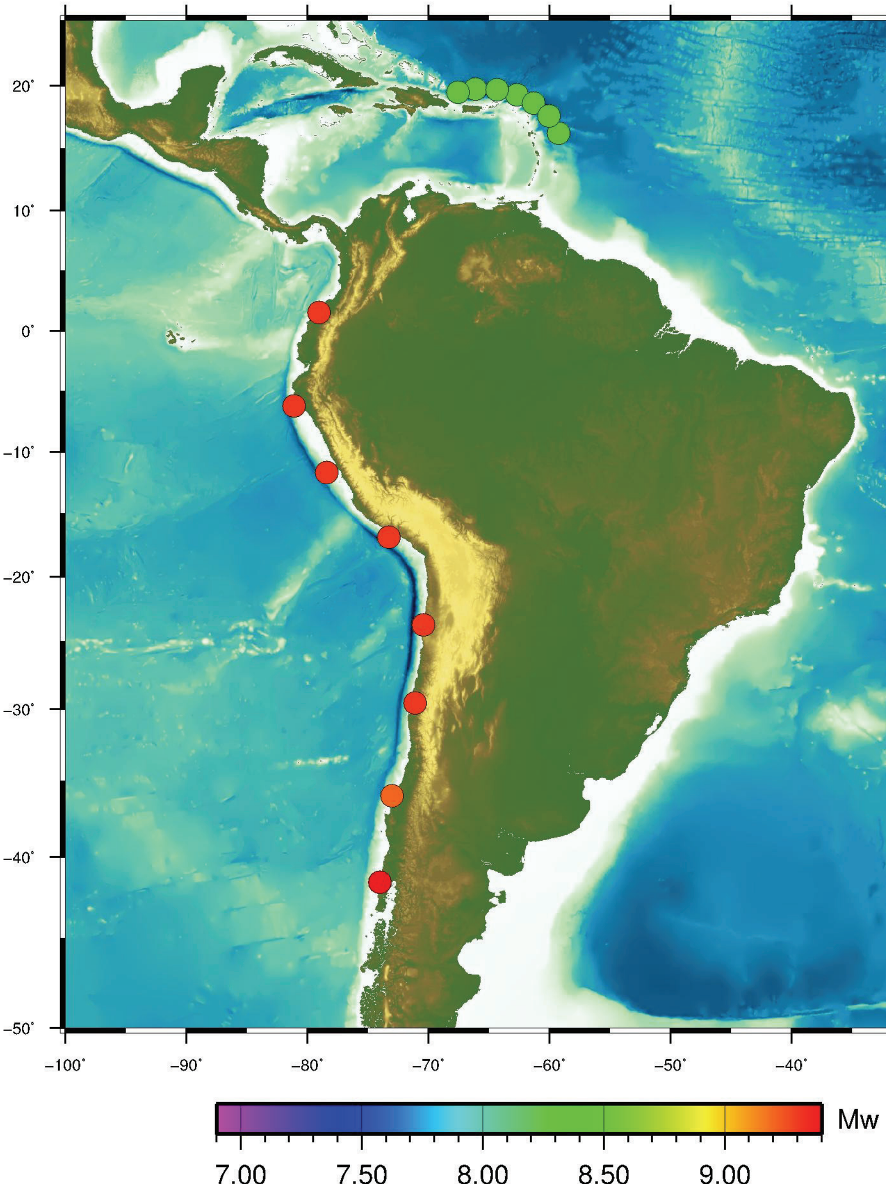

Figure 5 *Scenarios located along subduction zones offshore South America and the Caribbean*

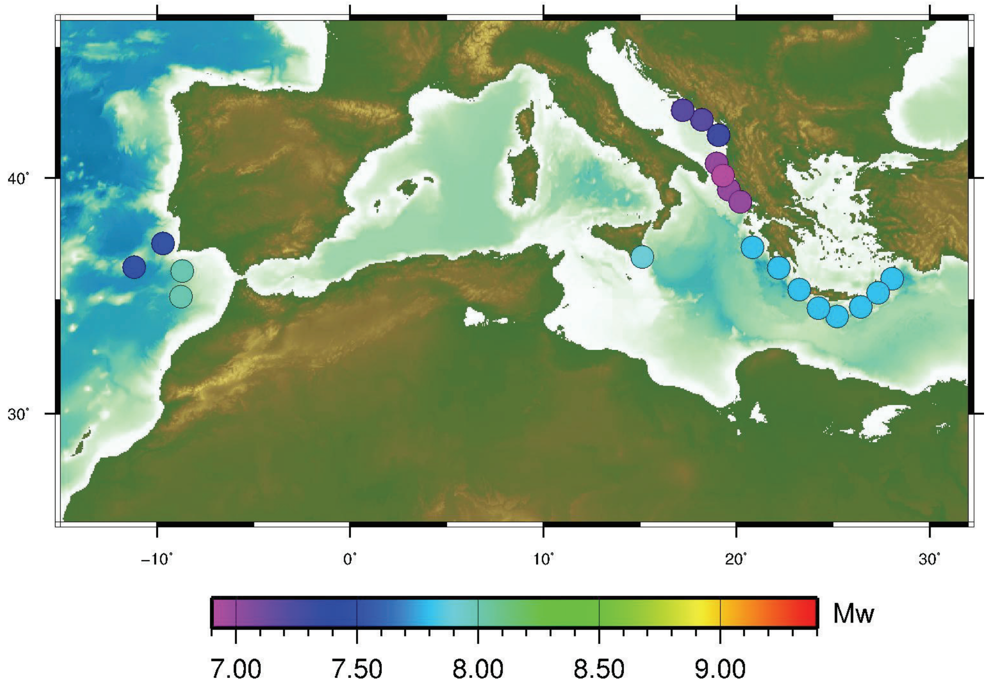

Figure B6 *Scenarios offshore Portugal and in the eastern Mediterranean. Note that the scenarios offshore Portugal is related to larger return periods and uncertainties with respect to focal mechanisms than the other scenarios.*

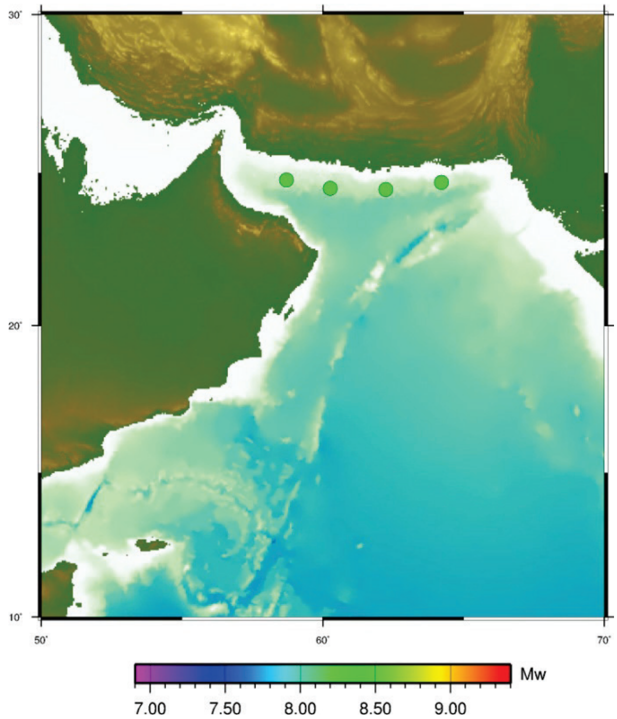

Figure B7 *Makran trench scenarios*

For the scenario earthquakes, earthquake faults of uniform width, length and slip are established, and in turn converted to seabed displacement using the standard analytical formula of Okada (1985). Smoothing due to the hydrodynamic response from the seabed dislocation is based on the formula of Kajiura (1963). For the subduction zone earthquakes where slip rates were obtained, the new scenarios were constructed assuming fault locking over 500 years. Convergence rates obtained from Bird (2003) are used. By using the scaling relations from Blaser et al. (2010), related magnitudes were found. By making assumptions on the fault shear strengths, related fault lengths and widths were in turn derived from the scaling. Typically the shear strengths were in the range of 20-40 GPa. Altogether this gives relatively conservative estimates for the scenario earthquakes. However, as discussed below, there are several other assumptions in the overall methodology that are non-conservative.

In certain areas where tectonics are more complex the slip rates and fault geometry are less easily obtained. Here, fault parameters are reproduced as accurately as possible from literature. As a consequence, the return periods are also less accurate. Yet, the return periods for these scenarios are assumed to be fairly similar to those originating from subduction zones. Literature data were used for Sicily (Tinti et al., 2012), the Adriatic Sea (Tiberti et al., 2008), eastern Indonesia (Løvholt et al., 2012b), and Cascadia (González et al., 2009). The scenarios offshore Portugal is motivated from the recent studies of Matias et al., (2013), aiming at a 500 year return period. It is noted that scenarios of similar magnitude of the 1755 earthquake and tsunami would imply return periods of several thousand years according to Matias et al., (2013). The scenarios offshore Portugal have different orientations, which reflect the uncertainty due to present lack of knowledge of the most likely focal mechanisms for megathrusts in this region.

B2.2 Wave propagation modelling

Near source and regional tsunami propagation are modelled using a linear dispersive wave model GloBouss (Pedersen and Løvholt, 2008; Løvholt et al., 2010), on publicly available ETOPO1 grids. For convergence, the grids are refined to the desired resolution by bi-linear interpolation. The maximum water level obtained from the time series at the control points is used to compute the further amplification to the shoreline as described in Section 2.4 of the surface elevation are extracted at near shore control points, and in turn the maximum water level is used. Totally over 10000 control points are applied, with an approximately spacing of 20 – 50 km. The control points are extracted automatically by a contouring algorithm (GMT, 2011) at a small reference depth of 50 meters. Inside the tsunami model the depth in the control point may deviate from the reference depth, so the surface elevation is normalized to 50 m by using Greens' law.

B2.3 Employed Probabilistic Tsunami Hazard Assessment method

The Probabilistic Tsunami Hazard Assessment (PTHA) approach describes the probability of exceedence for a given tsunami metric, and is derived from the well established method of Probabilistic Seismic Hazard Assessment (Cornell, 1968) but adapted to account for tsunami propagation. Relatively recent studies have applied the PTHA method to different regions, e.g. Geist and Parsons (2006) Annaka et al. (2007), Burbidge et al. (2008), Parsons and Geist (2009), and Thio et al. (2010). A short description of the employed PTHA method follows here, for a more complete description we refer to Horspool et al., (in prep).

The PTHA framework can be summarized as:

- Define tsunami sources (earthquake faults) to be included in the analysis.
- For each source discretize the fault into smaller sub-faults.
- For each source create a synthetic earthquake catalogue based on a recurrence model of choice (e.g. Gutenberg-Richter or Characteristic), which has probabilities associated with each earthquake.
- For each sub fault, calculate the unit seafloor deformation and propagate the tsunami from source to the control points at the reference depth.
- For each event in the catalogue, estimate the maximum water level at the near shore control point by summing the waves from all the individual sub faults that make up that event, and then scale by the amount of slip for that event.
- Combine the maximum water level from all sources to estimate the probability of exceedence.

The PTHA method was employed for the Indian Ocean and the South West Pacific. Tsunami megathrust sources around the western and northern Pacific Ocean, the Makran subduction, and the Sunda Arc were used. The subduction zone geometry and recurrence rates were taken from the PTHA for Australia (see i.e. Burbidge et al., 2008), which uses plate velocity vectors from GPS data to estimate the magnitude frequency distribution assuming full coupling on the plate interface. Sub faults for local crustal sources are 20km x 10km, whereas sub faults that are distant only are 100km x 50km.

In deep water the tsunami is linear, meaning that any tsunami can be constructed by the summation of the responses from the sub faults. Hence, the simulations are only carried out ones for the sub faults, and the hazard is determined by superpositioning. In the PTHA a linear finite difference model allowing for nesting formulated in geographical coordinates (Satake, 1995) is used for the simulation of the tsunami propagation for the unit sources. As for the worst case scenario simulations the maximum water elevation was extracted at the 50 m reference depth.

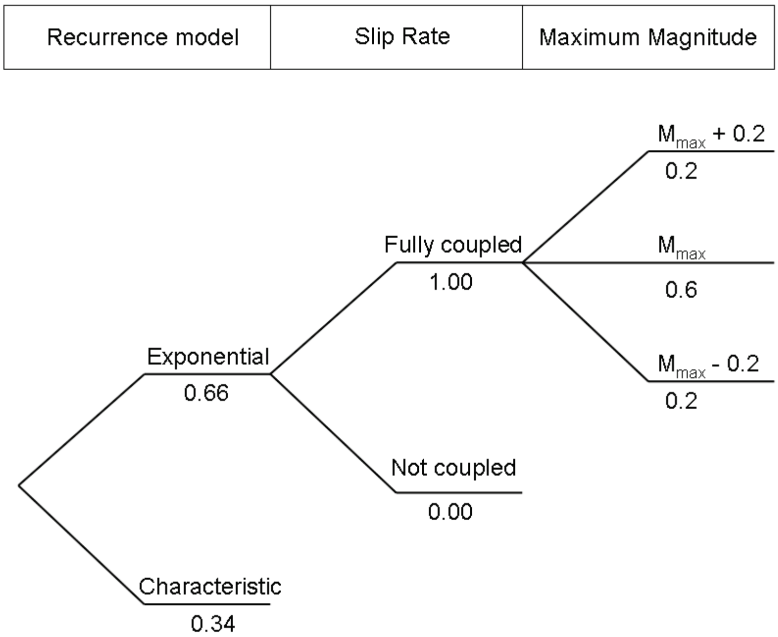

Figure B8 Outline of PTHA logic tree

Sources of epistemic uncertainty (uncertainties due to lack of knowledge) that are included in the PTHA are slip rate, earthquake recurrence model type, and maximum magnitude (Figure 8). Maximum magnitudes are constrained by scaling laws (Blaser et al., 2010). The maximum magnitude from the mean of the scaling laws is given a weighting of 0.6, and two alternative maximum magnitudes that are +0.2 magnitude units and -0.2 magnitude units from the best estimate, are given a weighting of 0.2. For each source, a truncated Gutenberg-Richter Magnitude Frequency Distribution (MFD) was given a weighting of 0.66 and a Characteristic Earthquake distribution was given a weighting of 0.34. A b-value of 1.0 is used for both MFD's. Main sources of aleatory uncertainty (inherent uncertainty) in the PTHA come from modelling uncertainties in source geometry, and random slip. The aleatory uncertainty was accounted for by summing up different variances from model errors, fault dip, and random fault slip. The uncertainties in dip and random slip were obtained from Monte Carlo simulations by varying the dip angle and employing the different slip realizations, respectively. Aleatory uncertainties were included by integrating across probability density functions.

Combining all the information from the sources and logic trees, a synthetic catalogue is generated which represents the full integration over earthquake magnitudes, locations and sources for every logic tree branch. The catalogue was generated by iterating through each magnitude in the MFD, and calculating the rupture dimensions using the scaling laws (Blaser et al., 2010). The rupture is then iteratively moved across the fault one sub fault at a time until that magnitude has occurred on every possible location within the fault dimensions. For M7.0 earthquakes on the subduction interface, the rupture dimensions are equal to one sub fault; therefore the number of ruptures would be equivalent to the number of sub faults. The maximum magnitude earthquake would occur once and rupture the whole fault if scaling laws have been used to constrain the maximum magnitude. This iterative process ensures that all magnitudes could occur at any possible location on the fault plane. For each event the probability of that magnitude was then weighted by one over the number of earthquakes represented by that magnitude. This ensures that the sum of the events of the same magnitude equals the annual probability of one event of that magnitude.

For each event in the synthetic catalogue, the tsunami hazard is calculated at each control point along the coast by summing the contributions from the sub faults that make up that event, and by scaling the tsunami height by the event slip. For each site, this results in a list of tsunami heights and associated annual probabilities. For a coherent description of the hazard compared to the worst case scenario simulations, maximum surface elevation from the PTHA for a return period of 500 years is given at near shore control points at the reference depth of 50 m. The further amplification to run-up is accounted for using the amplification factor method (Section 2.4). The present model assumes a Poisson process where earthquakes are independent and occur at a fixed rate over time.

B2.4 Run-up estimation and inundation mapping using amplification factors

To estimate tsunami run-up globally refined numerical inundation simulations are too time consuming. A faster procedure is to relate the nearshore surface elevations to the maximum shoreline water levels by using a set of amplification factors based on the parameters of the incident wave and the bathymetric slope. This procedure was developed for GAR 2009, and is described and validated in detail by Løvholt et al. (2012a), and only a part of the procedure is reviewed here.

The procedure is sketched in Figure 9. A range of different earthquake fault parameters are used to provide the set of initial conditions. These include the earthquake fault width (50, 100, 150, 200 km), and dip angle (5, 15, 20, 30 degrees), as well as inverting the polarity of the tsunami (leading trough or crest). The plane wave simulations are all run on idealized plane bathymetric configurations (see Løvholt et al., 2012a) where the shelf is broken up into two linear segments. From the plane wave simulations, factors for amplification that relate the surface elevation at time series gauges located at water depths of 50 m to the maximum shoreline water level are computed and stored in lookup tables. To determine the amplification factors along the idealized bathymetric profiles we apply a linear hydrostatic plane wave model. For smaller islands the plane wave assumption is severely violated, a 2HD model (GloBouss) must be applied. Both models apply a no-flux boundary condition at the shoreline leading to a doubling of surface elevation due to reflection. Although the models do not include dry land inundation, the surface elevation on the boundary close to the shoreline (at 0.5 m water depth) with a no-flux condition yields a good approximation. For long non-breaking waves, the linear solution for the run-up height at the shoreline and the non-linear solution for the run-up height on land are identical (Carrier and Greenspan, 1958). The validation of procedure is presented in Løvholt et al. (2012a). Based on Pedersen, (2011), we may further assume that the procedure should also provide reasonably accurate results for waves of moderately oblique incidence. For reviews of different methods for run-up estimation, see Synolakis et al., (2007), Pedersen (2008), and Løvholt et al., (2013).

To assign an amplification factor, an idealized bathymetric profile is manually assigned to each point. To estimate the maximum shoreline water level from the offshore time series gauges in a tsunami simulation, the amplification factor for a set of parameters is extracted from the lookup tables and in turn multiplied with the maximum surface elevation measured at the time series gauges.

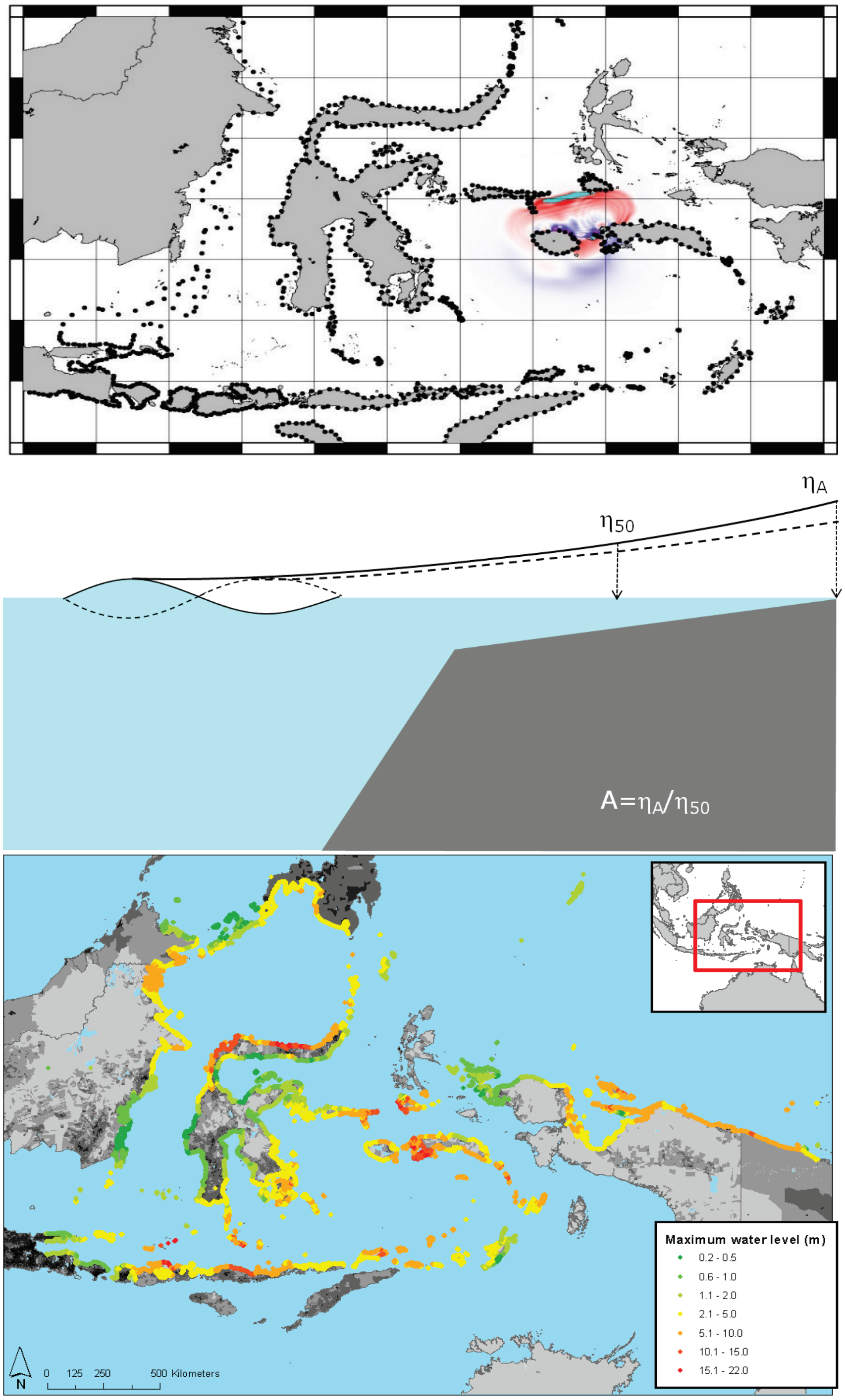

Figure B9 *Principles of the amplification factor method. Upper panel, regional tsunami simulation and locations of the time series gauges at the reference depth contour. Mid panel, sketch of an idealized bathymetric profile. The amplification factor is defined as the ratio between the water surface elevation at the shoreline over the water surface elevation at 50 m water depth. Lower panel, maximum shoreline water level obtained from superimposing results from a series of simulations.*

B2.5 Inundation mapping and exposure

Based on the maximum shoreline water levels, rough inundation maps were computed to count the population exposed to the tsunami. The inundated area was computed by first interpolating the water levels at the shoreline. An inverse distance weighted method was used to extrapolate the water elevations at the shoreline to the topographic contour maps. For the topographic data, the SRTM dataset was used. However, it turned out that for some very flat near shore locations, the inundation distance could be unreasonably high. To limit the inundation, a crude formula taking into account the head loss due to bottom friction was used. We represent the wave load at the shoreline by a constant surface elevation η and choose a friction coefficient $f=10^{-2}$. This friction is relatively high, slightly counterbalancing the conservative assumption of fault locking, yet providing reasonable inundation distances compared to real events. By assuming a quadratic friction law and a constant drop of hydraulic head loss along the inundation path, a simple formula for the maximum inundation distance L_{max} was obtained, proportional to the ratio of the surface elevation over the friction:

$$L_{\max} < \frac{\eta}{f}$$

The inundated areas represent 500 year return period hazard maps. The inundation maps are then overlaid on population exposure data (Landscan, 2007) and critical facility data for nuclear power plants (database provided by UNEP-GRID) and airports (http://www.ourairports.com/data/) to provide country wise and global statistics of the 500 year return period exposure. The total population exposure is found by integrating the Landscan data over the inundated area. Generally, the predicted inundation line intersects a Landscan grid cell. In this case, the exposed population is taken as the cell population times the inundated cell area over the total Landscan cell area. Only airports defined as medium and large were included in the statistics. Due to the limited accuracy of the inundation maps, three different categories were used in the exposure calculations for the critical facilities in order to take into account model uncertainty. The first category (Cat1) is a facility located in a potential inundated area. The second category (Cat2) is a facility located less than 1 km from the shoreline defined by the SRTM dataset. The third category (Cat 3) is a facility not exposed or not in area covered by this study.

B3 Results

Using GloBouss, the tsunami propagation was simulated for the 80 scenarios depicted in Figure 1. Examples of the simulated maximum water levels are depicted in Figure 10 through Figure 13. For each scenario, the maximum water level is found at the near shore control points, and the run-up is estimated using the amplification factors. As the control points are common for all scenarios, the largest of the maximum water levels are extracted from all scenario simulations. For the areas covered by the PTHA method, the exceedence amplitude for a return period of 500 years is reported.

Figure 14 shows the distribution of tsunami hazard globally from earthquake induced tsunamis. The analysis shows that populous Asian countries, most prominently Japan, but also China and Indonesia account for a large absolute number of people living in tsunami prone areas (Figure 15). This is due to the combination of large hazard and dense population. A similar hazard is found along the US and South American coastlines, but here the total exposure are smaller. In relative exposure, smaller countries like Macau and the Maldives are among the highest ranked countries. In these countries, a higher amount of the total population is exposed to tsunamis. Since tsunamis have a low probability of occurrence, Figure 15 provides the number of people living in tsunami-prone areas and not the average yearly exposure as provided for other hazards. Close-up of some locations are found in Figure 16, where examples of critical facilities such as nuclear power plants as well as airports close to or inside the tsunami hazard zone are given.

Examples of critical facilities that may be inundated by tsunamis include nuclear reactors and airports. Categories 1 and 2 are included in the statistics for both kinds of facilities. Figure 17 shows countries having nuclear power plants and reactors close to or within the inundated area. Japan has the largest number of nuclear power plants within the inundated area (7). When the nuclear power plants close (less than 1 km) to the shoreline is included, the United States has the largest total number (13). In Figure 18 the countries with the largest number of airports inside and close to the tsunami hazard zone are listed. Japan has the largest number of airports inside the hazard zone (24), while the United States have the largest total number including also those close the hazard zone (58). In certain areas such as the eastern United States and the United Kingdom, landslide induced tsunamis may constitute an additional significant threat towards critical facilities, but these tsunami sources are not included in the current statistics even though near shore critical facilities may in general be exposed to this additional threat.

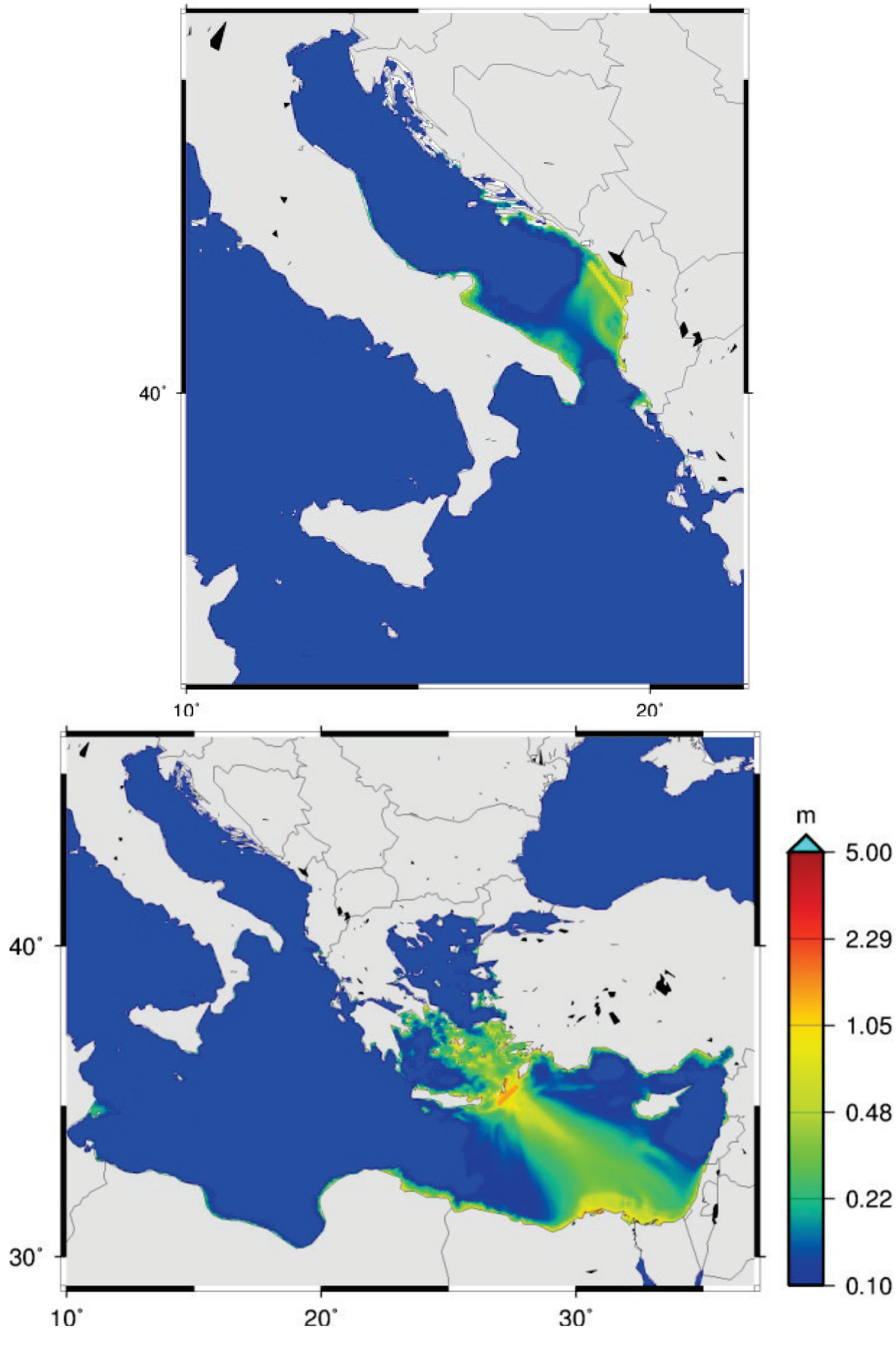

Figure B10 *Examples of simulated maximum water levels from two scenarios. Upper panel, example from the Adriatic Sea; lower panel, example from the Hellenic Arc. The colorbars indicate the maximum water level in meters.*

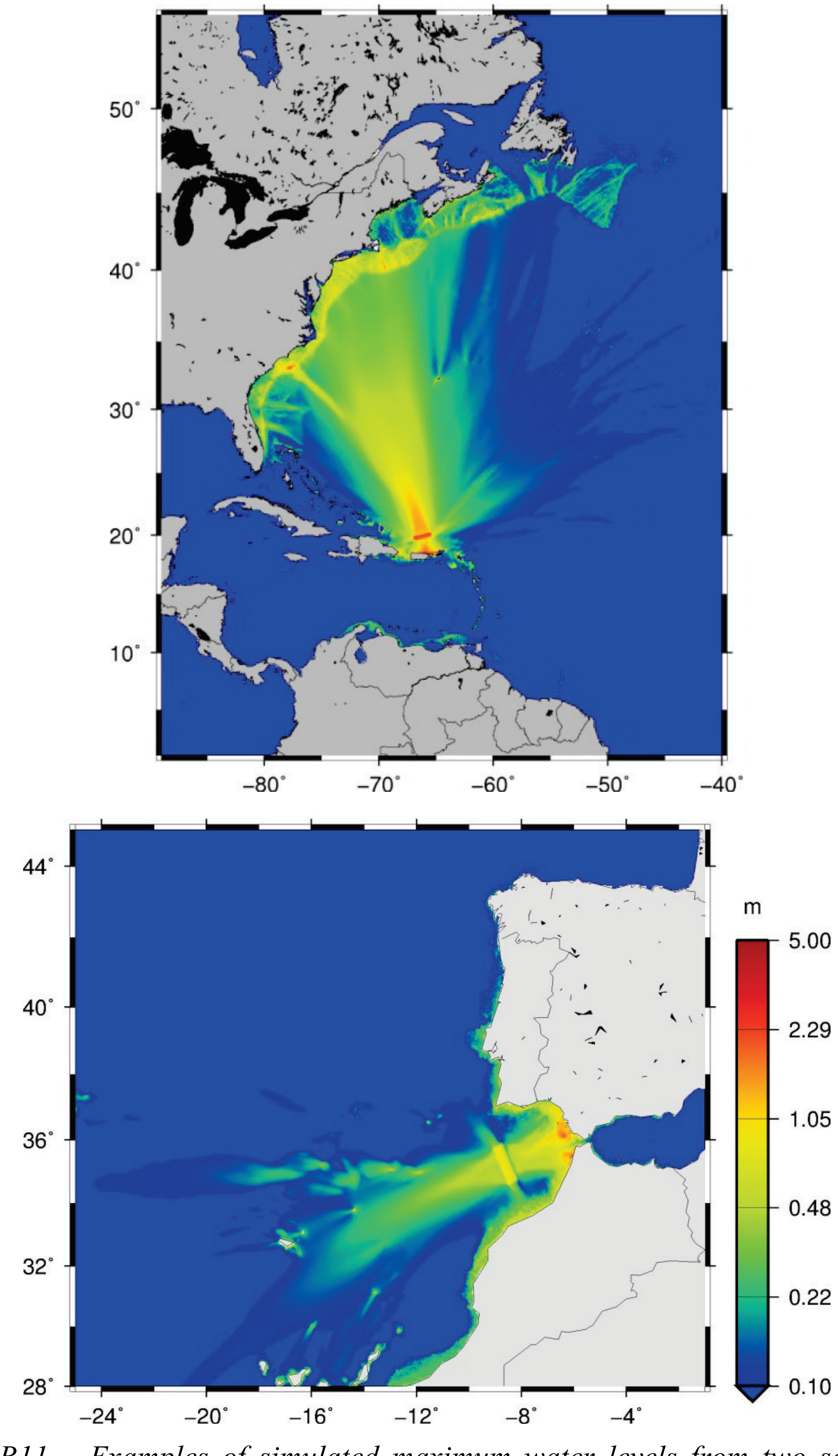

Figure B11 *Examples of simulated maximum water levels from two scenarios. Upper panel, example from the Puerto Rico trench; lower panel, example from offshore Portugal. The colorbars indicate the maximum water level in meters.*

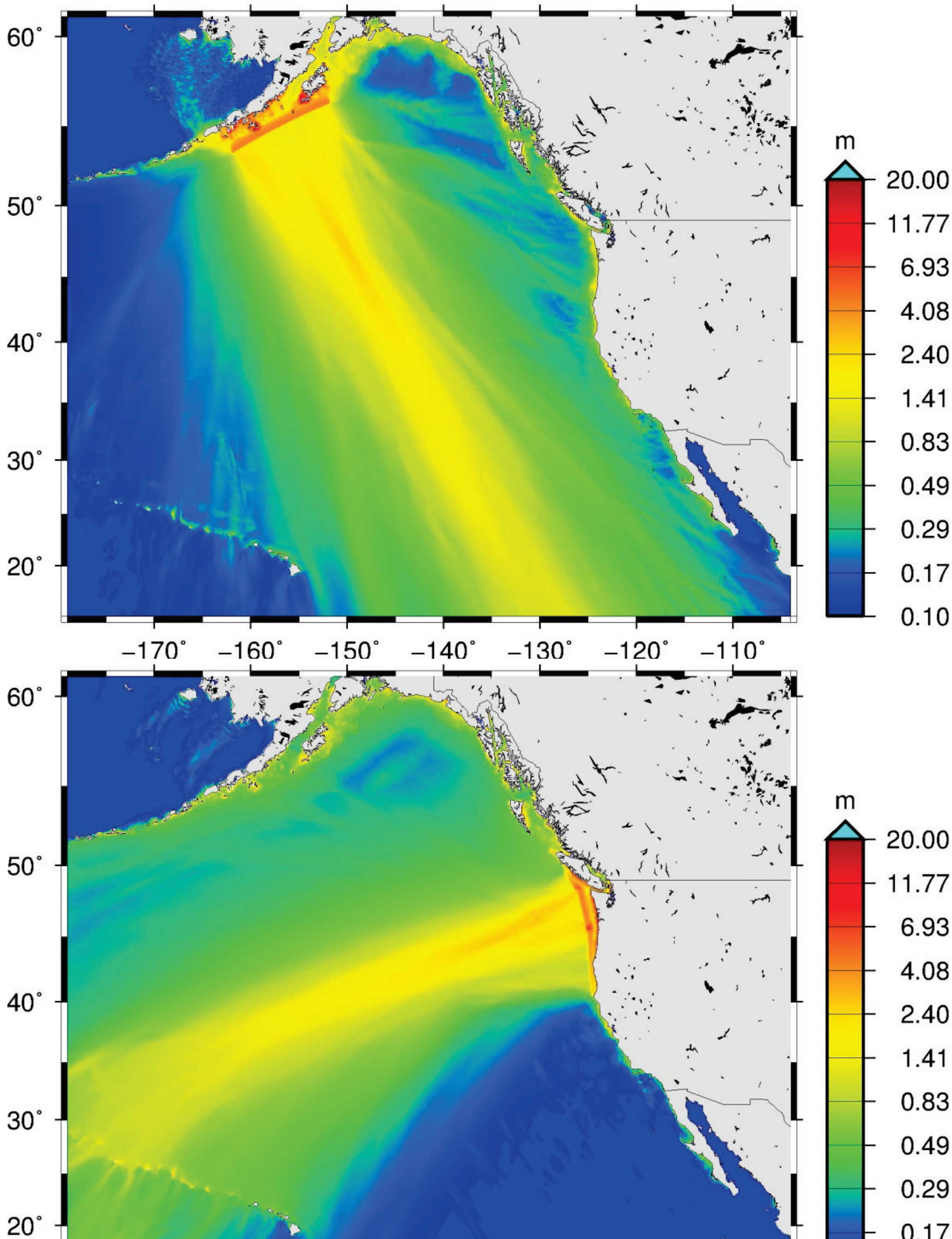

Figure B12 *Examples of simulated maximum water levels from two scenarios. Upper panel, example from Aleutian trench; lower panel, example from the Cascadia subduction zone. The colorbars indicate the maximum water level in meters.*

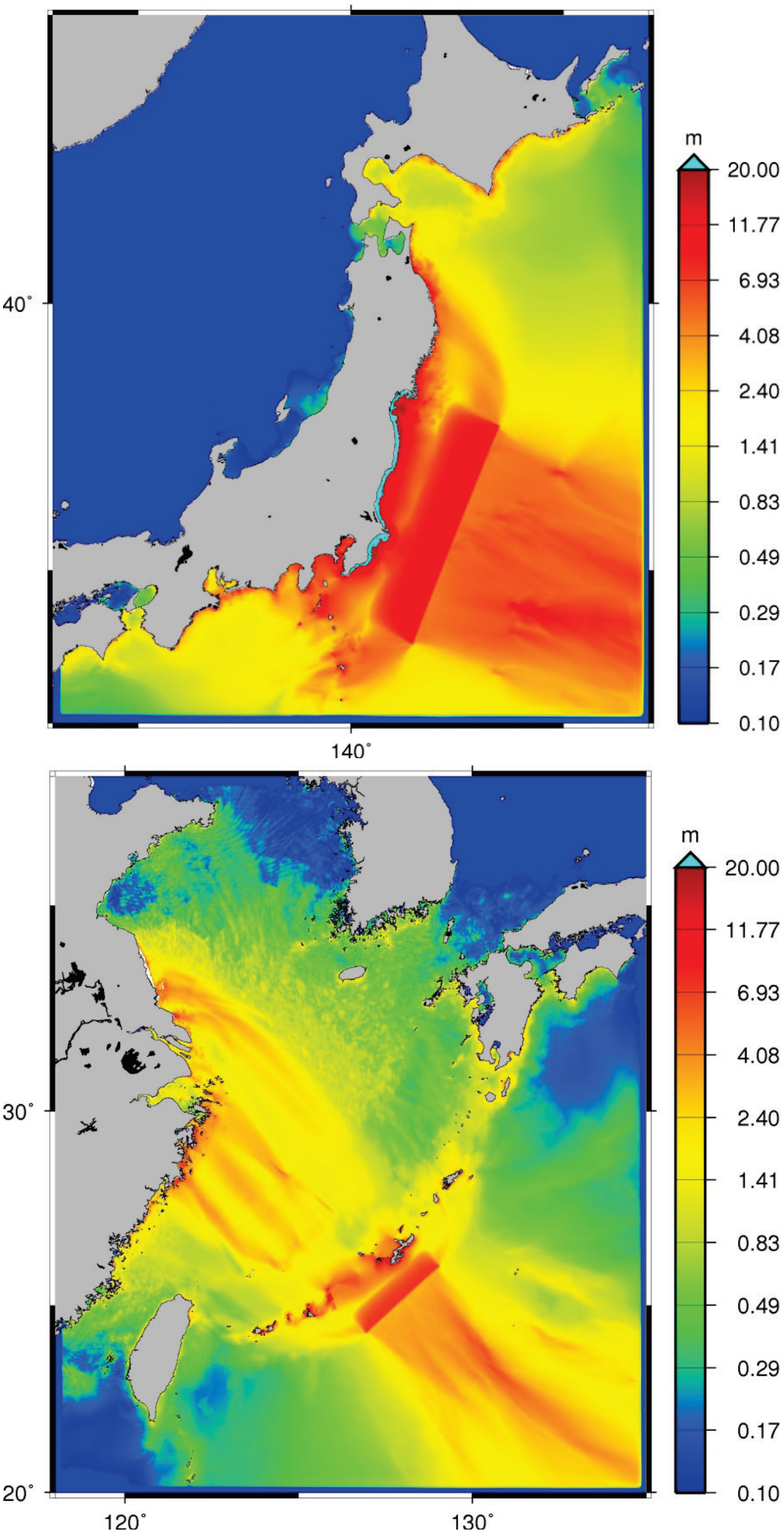

Figure B13 *Examples of simulated maximum water levels from two scenarios. Upper panel, example from the Japan trench; lower panel, example from the Ryukyu trench. The colorbars indicate the maximum water level in meters.*

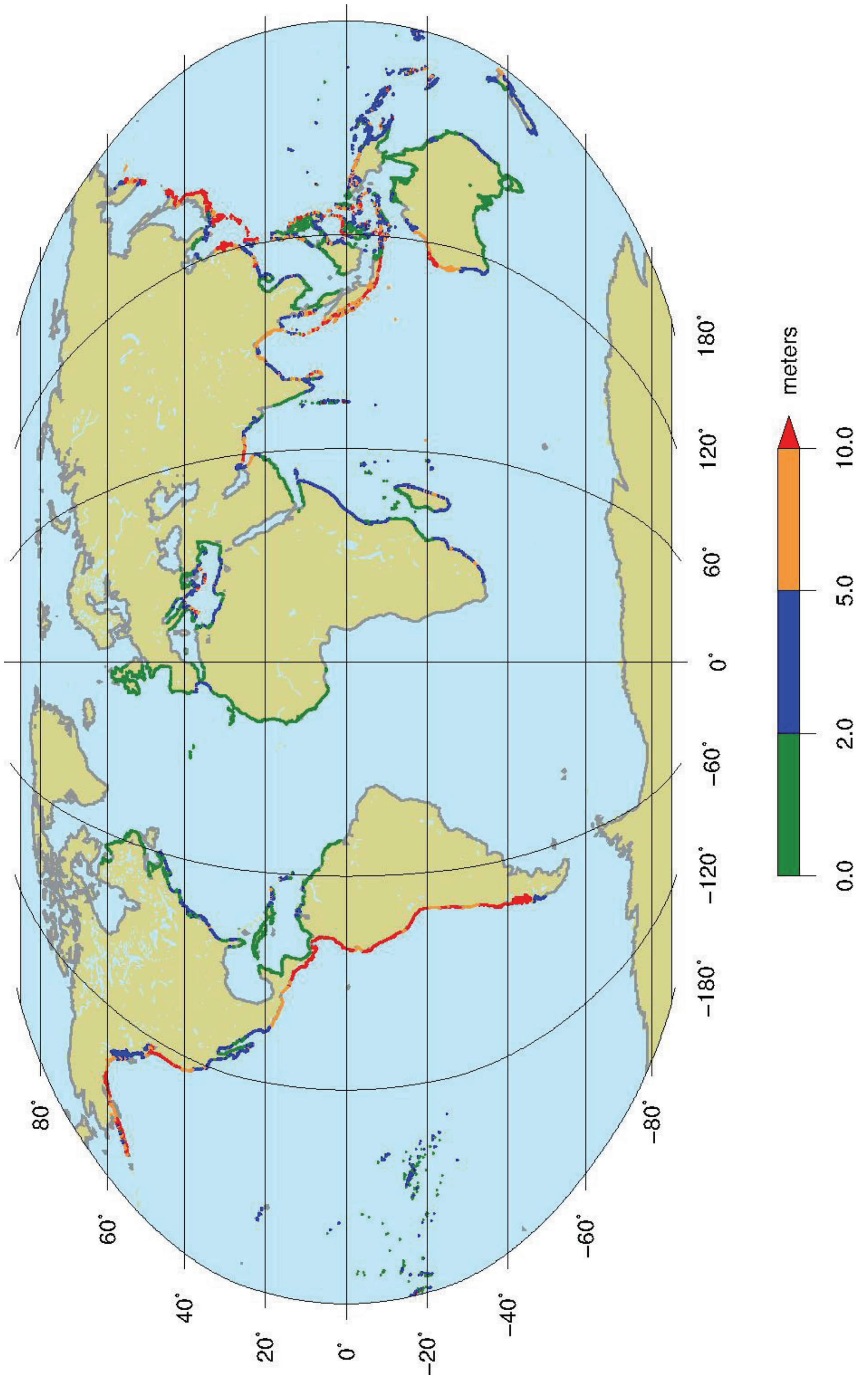

Figure B14 *Global tsunami hazard due to earthquakes for a 500 year return period. The color bar gives the maximum shore line water level in meters.*

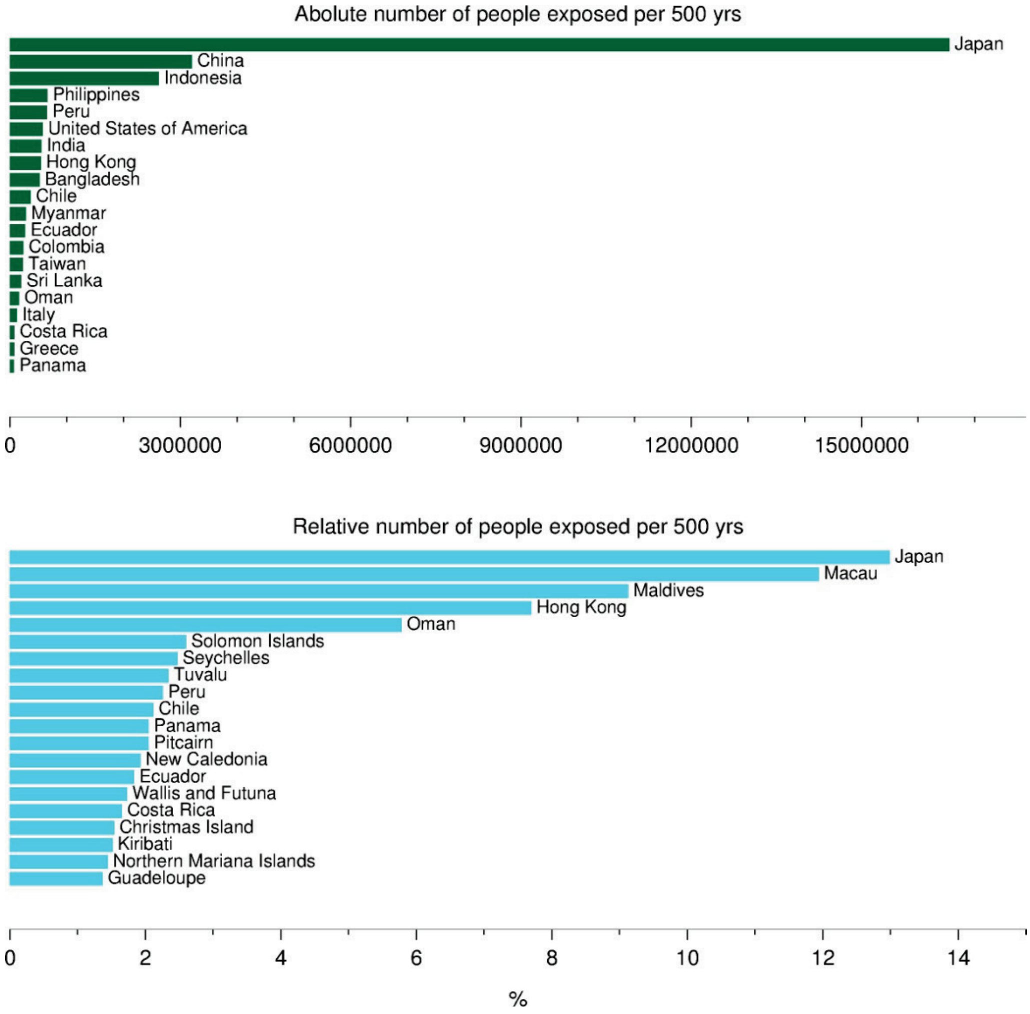

Figure B15 *Number of people living in areas potentially affected by tsunamis for a 500 year return period. The number of exposed persons divided by the total population in each country is given in percent in the lower panel.*

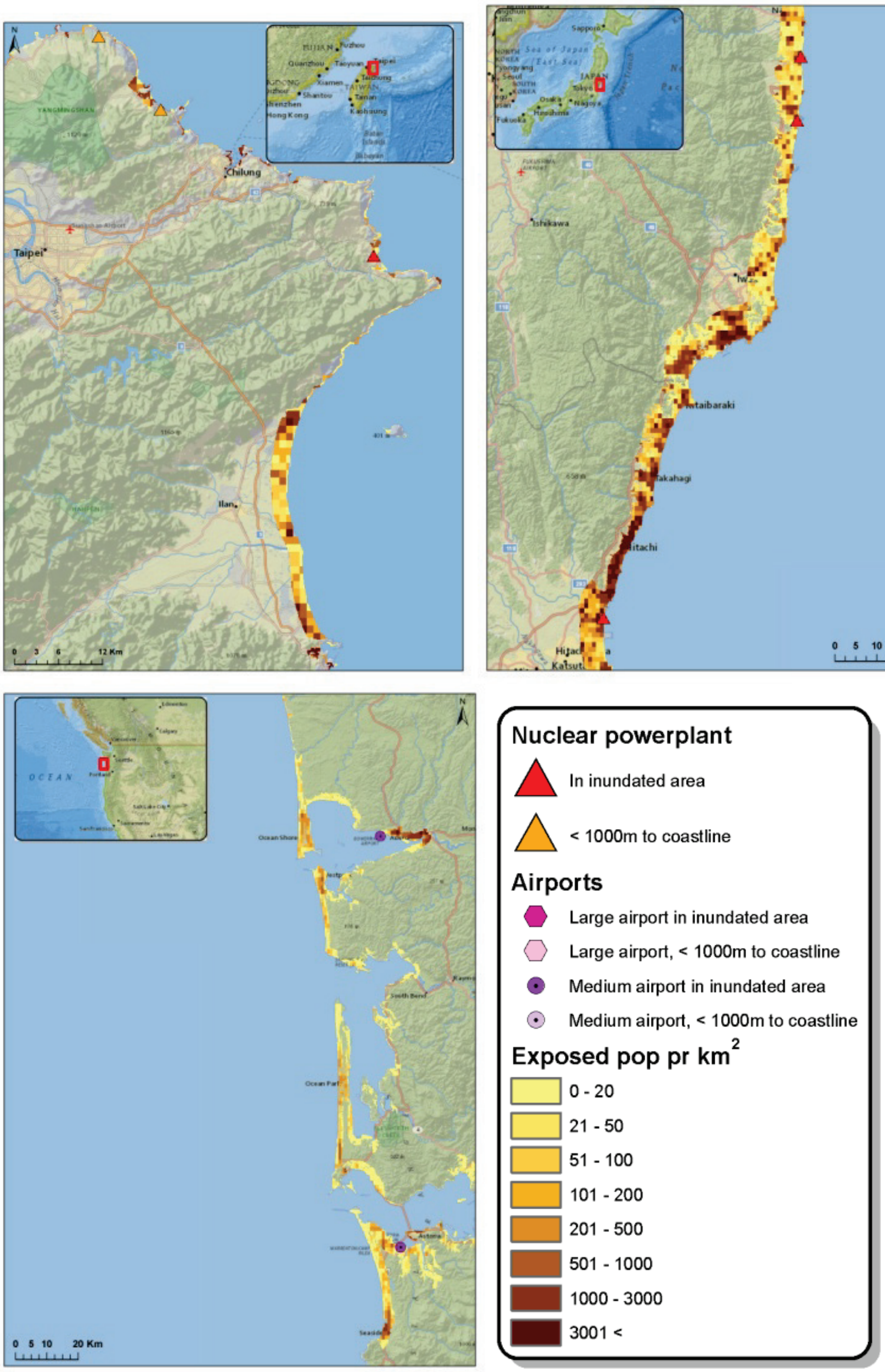

Figure B16 *Examples of tsunami exposure at northern Taiwan, eastern Japan, and western US coastline for a 500 year return period. Both population density and critical facility exposure are depicted.*

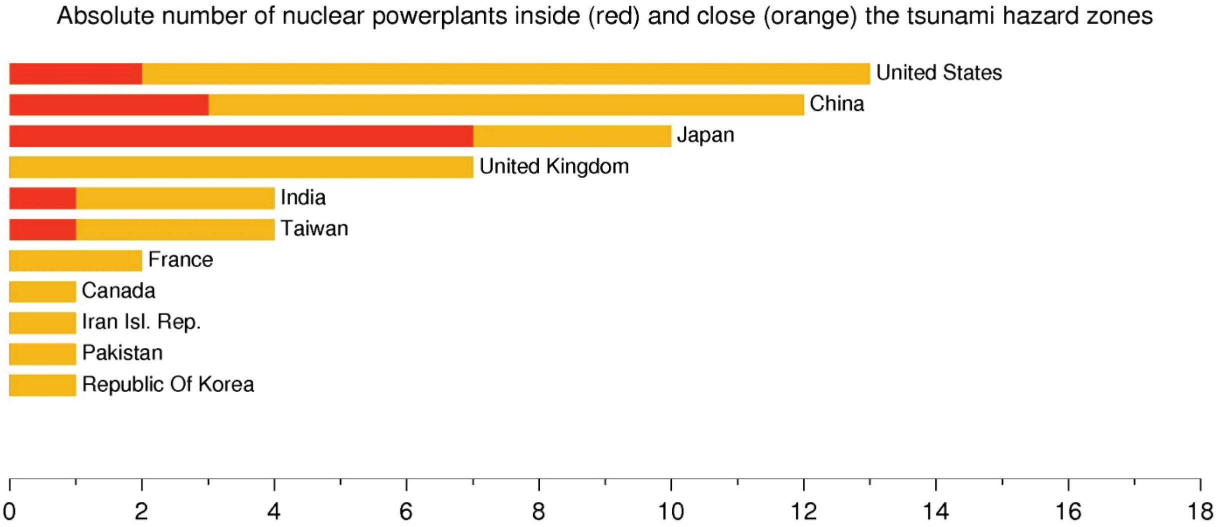

Figure B17 *Nuclear power plants close to or inside the tsunami inundation zone for a 500 year return period. The red color indicates number of nuclear power plants inside the tsunami hazard zone (Cat 1), while the orange color indicates the number of power plants closer than 1000 m to the tsunami inundation zone (Cat 2).*

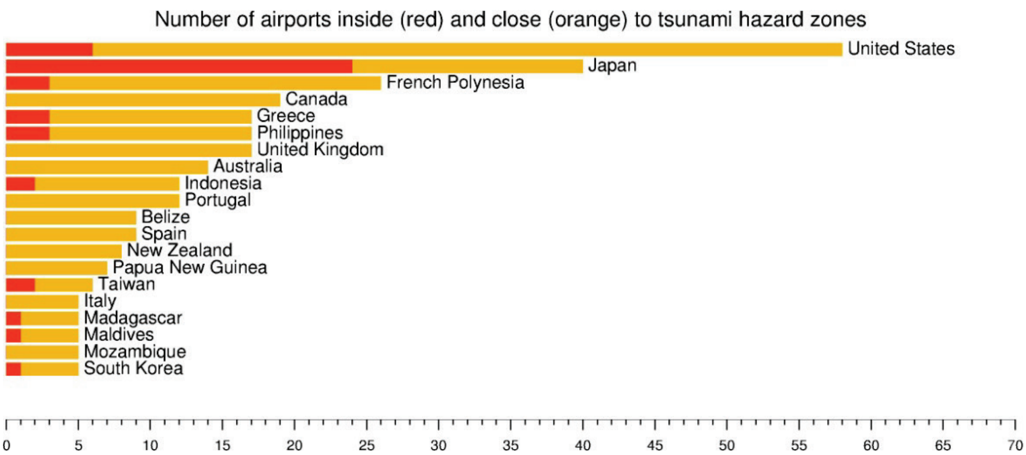

Figure B18 *Number of airports (large or medium) for (Cat 1, red) or closer than 1000 m (Cat 2, orange) to the tsunami inundation zone for a 500 year return period*

B4 Limitations, sources of error and look ahead

Below, the different limitations of the study are outlined. These partly address sources of error in the analysis, and partly the missing parts in the risk quantification. It is stressed that the results of the present analysis is deterministic, and although there are uncertainties related to the analysis, these are presently not quantified. Future updates of GAR will apply a probabilistic analysis (based on the PTHA method), and hence uncertainties will be addressed more quantitatively.

B4.1 Return periods

The largest and most destructive tsunami events like the 2004 Indian Ocean and 2011 Tohoku tsunami are generally posing larger risk to human lives than the smaller and more frequent events. For this first pass analysis, the tsunami hazard maps are focussing on extreme events only, that is, tsunamis generated by large earthquakes of return periods of approximately 500 years. It is noted that establishing the size of infrequently occurring earthquakes is uncertain due to the lack of a reliable long record. Hence, the return periods for the future tsunamis are not to be interpreted as precise estimates. We also remark that the assumption of a “memory free” fault and fault locking is conservative, as areas where recent large earthquakes have occurred may actually have a lower probability than the ones interpreted here. Still, due to the nature of the recent large earthquakes causing major tsunamis, it has been interpreted as necessary to provide conservative estimates of the scenario earthquake in order not to underestimate the hazard and risk.

Although earthquakes with a return period of roughly 500 years are often expected to provide the largest contribution to tsunami risk, earthquakes with both higher and smaller probabilities will contribute strongly. Megathrusts with return periods exceeding thousands of years, may imply much stronger tsunami sources than those provided here. In certain areas, such as for instance offshore Portugal, Spain, and Morocco, these may even be the risk driving events. Providing a range of tsunami return periods will therefore be necessary to more accurately estimate exposure and to quantify the risk.

B4.2 Non-seismic sources

It should also be noted that tsunamis generated by volcanoes, submarine landslides, rock slides and smaller earthquakes are not addressed in the present study. Non-seismic sources contribute to the generation of about one fifth of all tsunamis globally, and there are several examples of such tsunamis causing devastation, a recent example is the 1998 Papua New Guinea tsunami caused by a submarine landslide, killing 2182 people (source, http://www.emdat.be). In areas like eastern Indonesia (Løvholt et al., 2012b) and the Caribbean (Harbitz et al., 2012) tsunamis due to landslides and volcanoes are relatively more frequent, and contribute to a significant portion of the risk. It has also recently been claimed that large run-up in northern Japan following the 2011 Tohoku tsunami was induced by a huge submarine slump (Grilli et al., 2012). Unlike earthquakes, landslides are not constrained to the major subduction zones and may strike more surprisingly. Due to their source characteristics, they may generate larger run-up locally compared to earthquakes, but are generally less dangerous for the far field propagation (for a discussion of their hazard, see e.g. Harbitz et al., 2013). However, addressing their return periods is difficult.

B4.3 Interpretation of hazard maps and population exposure

Due to the extensive task of covering the whole world, emphasis is given to producing regional hazard maps and numbers for the exposure. The methods for establishing the hazard maps and population exposure are approximate and simplified meant to cover large geographical areas. They are not intended for detailed local hazard mapping, but rather to obtain regional and national exposure data for comparison with other hazards. It should be noted that inundation maps are based on coarse topographic data (SRTM) hampered with inaccuracies and falsely elevated land. This may lead to an underestimation of the inundation and therefore also the exposure. The effect is particularly pronounced in tropical areas (Römer et al., 2012), but may also play an important role in urban areas. Moreover, the effects of countermeasures such as breakwaters which are expected to decrease the exposure are not considered. Breakwaters are for instance common in Japan. In the hazard maps, differences in the reference height of the coastline sections are sometimes encountered. These differences may cause slight offsets between the affected zones and coastlines.

B4.4 Risk assessment

The tsunami risk may be defined as the product of the hazard, exposure, and vulnerability. The present study contains an analysis of the first two parts, while the vulnerability has not been addressed directly. To provide explicit comparison with other hazards, the tsunami risk needs to be quantified. Vulnerability and risk has not been quantified so far mainly for three reasons: A need to first prioritise tsunami hazard assessment and exposure as these are the primary input to a possible subsequent risk analysis; tsunami vulnerability has been sparsely studied prior to the Indian Ocean tsunami in 2004; vulnerability exhibits large local differences as demonstrated by the devastating tsunamis in 2004 and 2011; and reliable vulnerability models for present use do not exist. For instance, the lethality in Banda Aceh in 2004 was much higher than in Japan 2011 although the run-up heights were comparable. However, the economic loss was in turn much higher in Japan 2011 (http://www.emdat.be). How to interpret measures of vulnerability in future updates of GAR is not yet clear, but a future tsunami risk assessment should still be aimed at.

B5 References

Annaka, T., Satake, K., Sakakiyama, T., Yanagisawa, K., and Shuto, N. 2007. Logic-tree approach for probabilistic tsunami hazard analysis and its applications to the Japanese coasts. Pure Appl. Geophys. 164, 577-92.

Berryman et al., (2005): Review of Tsunami Hazard and Risk in New Zealand. Institute of Geological & Nuclear Sciences client report 2005/104

Bird, P. (2003). An updated digital model of plate boundaries. Geochem. Geophys. Geosyst., 4(3): 1027, doi:10.1029/2001GC000252.

Blaser, L., F. Krüger, M. Ohrnberger, and F. Scherbaum (2010), Scaling Relations of Earthquake Source Parameter Estimates with Special Focus on Subduction Environment, *Bull. Seis. Soc. Am.*, 100, 2914-2926

Burbidge, D., Cummins, P.R., Mleczko, R., and Thio H.K. (2008), A Probabilistic Tsunami Hazard Assessment for Western Australia, *Pure and Applied Geophysics*, DOI 10.1007/s00024-008-0421-x, 2008.

Carrier, G.F. and Greenspan, H.P. (1958), Water waves of finite amplitude on a sloping beach, J. Fluid Mech., 4 97-109

Cornell, C. A. (1968), Engineering seismic risk analysis, *Bull. Seismol. Soc. Am.*, 58, 1583–1606.

GAR, (2009), Global Assessment Report 2009, URL: http://www.preventionweb.net/english/hyogo/gar/2009/?pid:34&pif:3

Geist, E. and T. Parsons (2006): Probabilistic analysis of tsunami hazards. *Nat. Hazards*, 37, pp. 277-314.

GMT (2011), The Generic Mapping Tool, URL: http://gmt.soest.hawaii.edu/

González, F.I., E.L. Geist, B. Jaffe, U. Kânoğlu, H. Mofjeld, C.E. Synolakis, V.V. Titov, D. Arcas, D. Bellomo, D. Carlton, T. Horning, J. Johnson, J. Newman, T. Parsons, R. Peters, C. Peterson, G. Priest, A. Venturato, J. Weber, F. Wong, and A. Yalciner (2009), Probabilistic tsunami hazard assessment at Seaside, Oregon, for near- and far-field seismic sources. *J. Geophys. Res.*, 114, C11023, doi: 10.1029/2008JC005132

Grilli S.T., Harris, J.C., Tajali Bakhsh, T.S., Tappin, D.R., Masterlark, T., Kirby, J.T., Shi, F., Ma, G., (2012), Recent progress in the nonlinear and dispersive modelling of tsunami generation and coastal impact: Application to Tohoku 2011, 13èmes Journées de l´Hydrodynamique, 21-23 November 2012, Chatou, France

Harbitz,C.B., S. Glimsdal, S. Bazin, N. Zamora, F. Løvholt, H. Bungum, H. Smebye, P. Gauer, O. Kjekstad (2012), Tsunami hazard in the Caribbean: Regional exposure derived from credible worst case scenarios. *Continental Shelf Research* 8, 1-23, doi:10.1016/j.csr.2012.02.006.

Harbitz,C.B., F. Løvholt, and H. Bungum (2013): Submarine landslide tsunamis – how extreme and how likely? *Nat. Hazards, in press*

Horspool, N., Pranantyo, I., Griffin, J., Latief, H., Natawidjaja, D.H., Kongko, W., Cipta, A., Bustaman, Anugrah, S.D., and Thio H.K. (in prep) A Probabilistic Tsunami Hazard Assessment for Indonesia. *Submitted to Nat. Hazards Earth Syst. Sci.*

Kaistrenko, V.M., Pinegina, T., and Klyachko, M.A. (2003): Evaluation of tsunami hazard for the southern Kamchatka coast using historical and paleotsunami data. In Yalciner, Pelinovsky, Okal, and Synolakis (eds), Submarine Landslides and Tsunamis, 217-228, Kluver Academic Publishers

Kajiura, K. (1963), The leading wave of a tsunami, *Bull. Res. Inst.*, 41, 535–571.

LandScan, (2007). High Resolution Global Population Data Set © UT-Battelle, LLC, Operator of Oak Ridge National Laboratory, USA.

Løvholt, F., G. Pedersen, and S. Glimsdal, S., (2010), Coupling of dispersive tsunami propagation and shallow water coastal response, In Zahibo, N., Pelinovsky, E., Yalciner, A., and Titov, V. (eds.), *Proceedings of the "Caribbean Waves 2008" workshop in Guadeloupe Dec. 2008. The Open Oceanography Journal special volume.*

Løvholt, F., Glimsdal, S., Harbitz, C.B., Zamora, N., Nadim, F., Peduzzi, P., Dao, H., Smebye, H. (2012a) Tsunami hazard and exposure on the global scale, *Earth-Sci. Rev.*, 110, 1–4, 58-73, ISSN 0012-8252, 10.1016/j.earscirev.2011.10.002.

Løvholt, F., Kühn, D., Bungum, H., Harbitz, C.B., and Glimsdal, S. (2012b), Historical tsunamis and present tsunami hazard in eastern Indonesia and the southern Philippines, *J. Geophys. Res.*, 117, B09310, doi:10.1029/2012JB009425

Løvholt, F., Lynett, P., and Pedersen, G. (2013), Simulating run-up on steep slopes with operational Boussinesq models; capabilities, spurious effects and instabilities. *Nonlin. Pro. Geophys., in press*

Matias, L. M., Cunha, T., Annunziato, A., Baptista, M. A., and Carrilho, F.: Tsunamigenic earthquakes in the Gulf of Cadiz: fault model and recurrence, *Nat. Hazards Earth Syst. Sci*., 13, 1-13, doi:10.5194/nhess-13-1-2013, 2013

Nadim, F. and Glade, T.: On tsunami risk assessment for the west coast of Thailand, F. Nadim, R. Pöttler, H. Einstein, H. Klapperich, and Ste Kramer (Eds), ECI Symposium Series, 7. http://services.bepress.com/eci/geohazards/28, 2006.

Okada, Y. (1985): Surface deformation due to shear and tensile faults in a half-space. *Bull. Seismic Soc. of Am*. 74, 4, pp. 1135-1154.

Synolakis, C.E. Bernard, E.N., Titov, V.V., Kânoglu, U., and Gonzaléz, F. (2007), Validation and Verification of Tsunami Numerical Models, *Pure Appl. Geophys.* 165, 2197–2228

Parsons, T., and Geist, E., 2009. Tsunami probability in the Caribbean Region. *Pure and App.Geoph.* 165: 2089-2116

Pedersen, G., (2008). Modeling run-up with depth integrated equation models. *In Advanced Numerical Models for Simulating Tsunami Waves and Run-up*, Liu, P.L.-F., Yeh, H., and Synolakis, C. 3-41. World Scientific

Pedersen, G. and Løvholt, F. (2008), Documentation of a global Boussinesq solver, *Preprint Series in Applied Mathematics 1*, Dept. of Mathematics, University of Oslo, Norway

Pedersen, G. (2011), Oblique runup of non-breaking solitary waves on an inclined plane, *J. Fluid Mech.*, 668, 582–606, doi:10.1017/S0022112010005343

Römer, H., Willroth, P., Kaiser, G., Vafeidis, A.T., Ludwig, R., Sterr, H. and Revilla Diez, J. (2012), Potential of remote sensing techniques for tsunami hazard and vulnerability analysis – a case study from Phang-Nga province, Thailand, *Nat. Hazards Earth Syst. Sci.*, 12, 2103-2126

Satake, K., (1995) Linear and non-linear computations of the 1992 Nicaragua earthquake tsunami. *Pure and Applied Geophysics*, 144, 455-470.

Stein, S., and Okal, E.A, (2007), Ultralong Period Seismic Study of the December 2004 Indian Ocean Earthquake and Implications for Regional Tectonics and the Subduction Process, *Bull. Seism. Soc. Am.*, 97, S279–S295, doi:10.1785/0120050617

Tiberti, M.M., Lorito, S., Basili R., Kastelic, V., Piatanesi, A., and Valensise, G. (2008), Scenarios of Earthquake-Generated Tsunamis for the Italian Coast of the Adriatic Sea, *Pure Appl. Geophys*. 165, 2117–2142

Tinti S., Armigliato A., Zaniboni F., Pagnoni G. (2012), Influence of the heterogeneity of the seismic source on the timely detectability of a tsunami: implications for tsunami early warning in the central Mediterranean. *Proceedings of the 22nd International and Polar Engineering Conference*, ISOPE-2012, Rhodes, June 17-22, 2012.

Thio H.K., Somerville P., and Polet J., (2010), Probabilistic Tsunami Hazard in California, *PEER Report 2010/108* Pacific Earthquake Engineering Research Center

Kontroll- og referanseside/
Review and reference page

NGI

Dokumentinformasjon/*Document information*

Dokumenttittel/*Document title* UNISDR Global Assessment Report 2015 - GAR15 Tsunami methodology and results overview	**Dokument nr/***Document No.* 20120052-03-R
Dokumenttype/*Type of document* ☒ **Rapport/***Report* ☐ **Teknisk notat/***Technical Note* **Distribusjon/***Distribution* ☒ **Fri/***Unlimited* ☐ **Begrenset/***Limited* ☐ **Ingen/***None*	**Dato/***Date* 28 May 2014 **Rev.nr./***Rev.No.* 1, 6 February 2015
Oppdragsgiver/*Client* The United Nations Office for Disaster Risk Reduction – UNISDR	
Emneord/*Keywords* Tsunami, hazard assessment, PTHA, Global study, inundation mapping	

Stedfesting/*Geographical information*

Land, fylke/*Country, County*	**Havområde/***Offshore area*
Kommune/*Municipality*	**Feltnavn/***Field name*
Sted/*Location*	**Sted/***Location*
Kartblad/*Map*	**Felt, blokknr./***Field, Block No.*
UTM-koordinater/*UTM-coordinates*	

Dokumentkontroll/*Document control*

Kvalitetssikring i henhold til/*Quality assurance according to* **NS-EN ISO9001**

Rev./ *Rev.*	**Revisjonsgrunnlag/***Reason for revision*	**Egenkontroll/** *Self review* **av/by:**	**Sidemanns-kontroll/** *Colleague review* **av/by:**	**Uavhengig kontroll/** *Independent review* **av/by:**	**Tverrfaglig kontroll/** *Inter-disciplinary review* **av/by:**
0	Original document	2014-05-28 Finn Løvholt	2014-05-28 Carl Harbitz		2014-05-28 Carl Harbitz
1	Revision 1	2015-02-06 Finn Løvholt			2015-02-06 Carl Harbitz

Dokument godkjent for utsendelse/ *Document approved for release*	**Dato/***Date*	**Sign. Prosjektleder/***Project Manager*
	2015-02-06	Farrokh Nadim

NGI er et internasjonalt ledende senter for forskning og rådgivning innen geofagene. Vi utvikler optimale løsninger for samfunnet, og tilbyr ekspertise om jord, berg og snø og deres påvirkning på miljøet, konstruksjoner og anlegg.

NGI arbeider i følgende markeder: olje og gass, bygg og anlegg, samferdsel, naturskade og miljøteknologi.

NGI er en privat stiftelse med kontor og laboratorier i Oslo, avdelingskontor i Trondheim og datterselskap i Houston, Texas, USA.

NGI ble utnevnt til "Senter for fremragende forskning" (SFF) i 2002, og leder "International Centre for Geohazards" (ICG).

www.ngi.no

NGI is a leading international centre for research and consulting in the geosciences.

NGI develops optimum solutions for society, and offers expertise on the behaviour of soil, rock and snow and their interaction with the environment, installations and structures.

NGI works within the oil and gas, building and construction, transportation, natural hazards and environment sectors.

NGI is a private foundation with office and laboratory in Oslo, branch office in Trondheim and daughter company in Houston, Texas, USA. NGI was awarded Centre of Excellence status in 2002, and leads the International Centre for Geohazards (ICG).

www.ngi.no

Hovedkontor/Main office:
PO Box 3930 Ullevål Stadion
NO-0806 Oslo
Norway

Besøksadresse/Street address:
Sognsveien 72, NO-0855 Oslo

Avd Trondheim/Trondheim office:
PO Box 1230 Pirsenteret
NO-7462 Trondheim
Norway

Besøksadresse/Street address:
Pirsenteret, Havnegata 9, NO-7010 Trondheim

T: (+47) 22 02 30 00
F: (+47) 22 23 04 48

ngi@ngi.no
www.ngi.no

Kontonr 5096 05 01281/IBAN NO26 5096 0501 281
Org. nr/Company No.: 958 254 318 MVA

BSI EN ISO 9001
Sertifisert av/Certified by BSI, Reg. No. FS 32989